× 80 μm rectangular areas were selected, excluding those in which retinal vessels had a cone mosaic that required degrading. Bright spots 2–5 μm in diameter were considered to be cones. A single examiner (KB) manually marked the cones in the target area. The examiner used the accented edges function of Photoshop CS1 whenever this function made the task easier. However, even when this function was used, the final identification of the cone was always done by observing the original averaged image.

Results

In both the volunteers and the patient, the ocular aberration was reduced to below 0.1 μm RMS (Table 1). In the two normal subjects, the photoreceptors were imaged as slightly oval-shaped bright dots with a tiled packing arrangement (Fig. 3; the AO image of normal subject 2 is not shown). The diameter of the bright dot was approximately 4 μm, and the density was 40950/mm^2 and 54530/mm^2 at 2° from the fovea centralis. These values are comparable to those obtained by another histological study of the human cone mosaic (40000–50000/mm^2).[12]

In the eye with macular dystrophy, the visual field obtained by the SLO microperimetry showed a ring scotoma. The fixation point was located within the bull's eye lesion and was approximately 200 μm superonasal from a central dark area (Fig. 2). The OCT images showed cystic changes in the fovea and degenerative changes of the retinal pigment epithelium in the macular area, but the precise degree of photoreceptor degeneration could not be determined.

In the AO retinal image, the observed morphology of the photoreceptor layer varied considerably, suggesting degeneration of the photoreceptors (Fig. 4). No structure was observed in the central dark area, and the shape of the white dots in the surrounding bright-colored area varied widely (Fig. 4A). Relatively uniform white dots were observed at several loci in the same area.

In the area where the white dots were uniformly distributed, the distance between spots was 3–4 μm, comparable

Table 1. Profiles of subjects

	Normal 1	Normal 2	Patient
Sex	Male	Female	Male
Age (years)	38	31	40
Imaged eye	OS	OS	OS
Retinal status	No disease	No disease	Macular dystrophy
BCVA	20/15	20/20	20/60
Subjective refraction	Sph-1.0 D Cyl-0.3 D	Sph-0.9 D Cyl-0.2 D	Sph-1.8 D Cyl-0.8 D
RMS[a] without AO (μm)	0.317	0.213	0.306
RMS with AO (μm)	0.083	0.078	0.094
Average cone density[b] (cones/mm^2)	40950	54530	ND

BCVA, best-corrected visual acuity; RMS, root mean square; AO, adaptive optics; ND, not done.

[a]Root mean square value of aberration coefficients of the second to eighth Zernike order for a 5-mm pupil diameter. The 2° temporal from the fovea was measured.

[b]Calculated from the cone spacing in the area 2° temporal from the fovea.

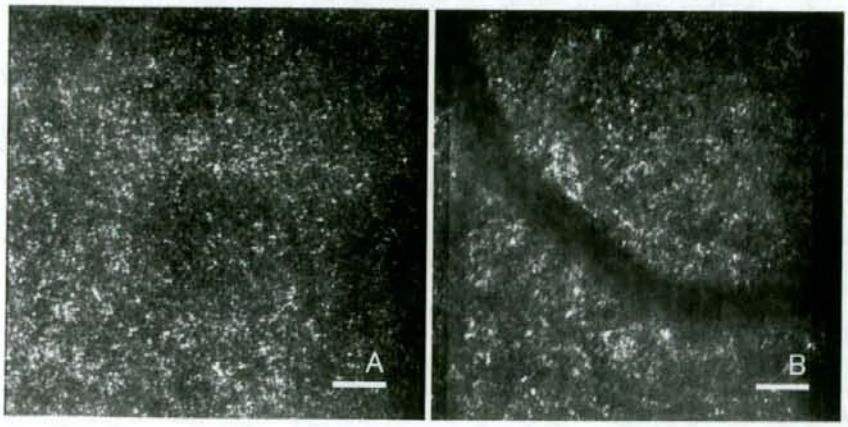

Figure 3A, B. AO image of a normal subject. Deconvolution was performed by using residual wavefront error data and subsequently five frames were averaged. **A** Center of the macula. The image covers the foveal avascular zone. The foveal center appears relatively darker than the surrounding area. **B** Three degrees temporal to the foveal center. Bar = 50 μm.

Jpn J Ophthalmol
Vol 52: 380–385, 2008

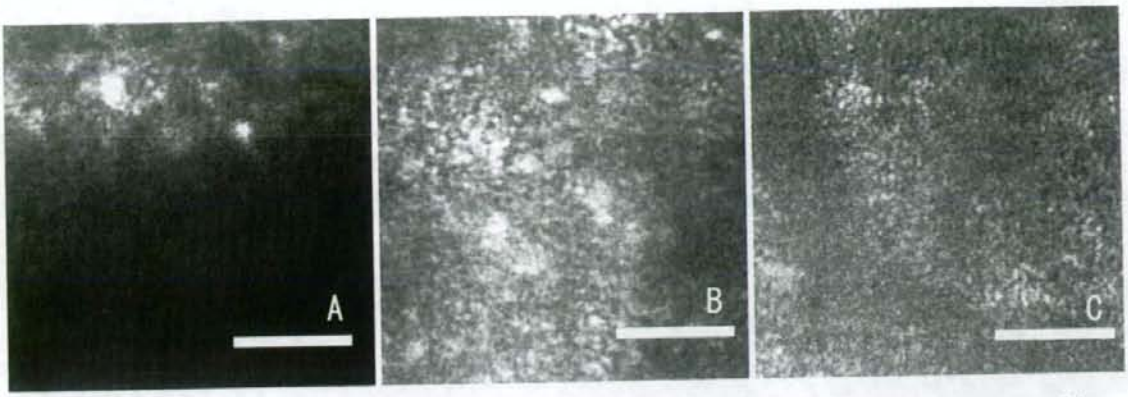

Figure 4A–C. Individual AO images of the sampled areas. The orientation of each image was determined by creating a composite AO image and registering it on the color fundus picture in Fig. 2. The letters correspond to the labeled sampling areas in Fig. 2. The total residual root mean square wavefront error was 0.089, 0.090, 0.162 μm for **A–C**, respectively, for a 5-mm pupil. **A** Upper edge of the central dark area. Very large irregular spots are seen above the dark area. **B** Example of an image with large, scattered, irregular spots. **C** Area near the locus of fixation. The dark vertical streak represents a capillary vessel. A patchy dark area is also seen on the right side of the image. Bar = 50 μm.

to that in the normal eyes and consistent with the interphotoreceptor distance obtained from histological data.[12]

In the nonuniform area, the bright spots were larger, ranging from 2 to 20 μm, and less uniform than those in the normal retinas, in which photoreceptors appeared as uniform small spots of 2–5 μm (Fig. 4B).[12] In the fixation area, the spots were more uniform in size and the overall appearance was more similar to normal retinas (Fig. 4C).

Discussion

The AO system used in this study is equipped with an LCPM as a wavefront corrector instead of the deformable mirror used in other AO systems. In our previous study we showed that this compact AO system can still effectively resolve cone photoreceptors. On the other hand, the LCPM has several limitations. The current system operates at approximately 3 Hz; thus, eye movement can affect the image quality. In this study, all subjects, including the macular dystrophy patient, had good fixation as judged from the AO images in the movie sequence, so the eye movement may not have been significant. We selected a 690-nm laser diode as the illuminator in order to reduce glare during the examinations. Because the coherence of this illuminator causes speckles, we used a rotating diffuser. Another problem may be that the LCPM can modulate only polarized light. This means that with this system we could obtain only partial optical information from the retina, which might be a problem when precise optical properties of retinal microstructures are studied, but we believe that the system is still applicable to the study of two-dimensional photoreceptor arrangements or photoreceptor morphology.

In the normal subjects, it was possible to obtain clear images of the photoreceptors with good wavefront compensation (Fig. 2). In this study, the calculated size of each spot was 2–5 μm, consistent with that obtained by other studies using a high-resolution system[13] or OCT[14] and by histological studies.[12]

In the eye with macular dystrophy, several patterns of AO image were seen in the bull's eye lesion. A central dark-colored area was uniform without structure. This may indicate either that a disorder of the inner retinal layers blocked the image or that the photoreceptors in this area are absent.

In the surrounding rough bright-colored area, scattered white spots of different shapes and sizes were seen. As this area showed reduced retinal sensitivity in SLO microperimetry, these spots may represent either morphologically changed photoreceptors or photoreceptor degeneration debris (Fig. 4).[8]

The fixation point on the retina was also located in the surrounding rough bright-colored area. The AO image showed a rather uniform distribution of white spots whose separation was consistent with the cone mosaic. It is possible that the photoreceptors were less affected in the fixation area.

The image obtained using the AO system is not fully understood. The spots in the AO images might be inner segment–outer segment (IS/OS) photoreceptor junctions because in the normal retina each spot seems to be in a one-to-one correspondence with a single photoreceptor, and because recent studies using high-resolution OCT suggest that the IS/OS junction seems to show its highest reflectivity inside the photoreceptor layer.[15] At the same time, it has been observed that this IS/OS reflection tends to disappear and reappear during the course of retinal diseases such as serous macular detachment[16] or macular hole, indicating that the IS/OS reflection probably indicates a functional aspect of the photoreceptors and that loss of the IS/OS reflection does not necessarily mean the absence of

the photoreceptor itself. Considering this, we note that the absence of regular spots does not necessarily mean the absence of photoreceptors, but it may indicate a functional change in the photoreceptors. In the same way, irregular spots, too, may be signs of a functional change in the photoreceptors. It may be possible to learn more about this issue by a study combining AO fundus camera and high-resolution OCT images.

Although our AO system has several limitations, we have shown that a two-dimensional image of photoreceptor cells can be obtained that is useful for examining macular dystrophy. In the future, animal studies are needed to investigate the origin of the large spots, and studies to improve the resolution of the AO system for quantitative evaluation of residual photoreceptors in diseased retinas are also needed.

Acknowledgments. Kenichiro Bessho and Takashi Fujikado had full access to all data in the study and take responsibility for the integrity of the data and the accuracy of the data analysis. This study was supported by a Health Sciences Research Grant (H19-sensory-001) from the Ministry of Health, Labour and Welfare, Japan

References

1. Liang J, Williams DR, Miller DT. Supernormal vision and high-resolution retinal imaging through adaptive optics. J Opt Soc Am A 1997;14:2884–2892.
2. Roorda A, Williams DR. The arrangement of the three cone classes in the living human eye. Nature 1999;397:520–522.
3. Roorda A, Romero-Borja F, Donnelly WJ III, et al. Adaptive optics scanning laser ophthalmoscopy. Opt Express 2002;10: 405–412.
4. Hermann B, Fernandez EJ, Unterhuber A, et al. Adaptive-optics ultrahigh-resolution optical coherence tomography. Opt Lett 2004;29:2142–2144.
5. Doble N, Yoon G, Chen L, et al. Use of a microelectromechanical mirror for adaptive optics in the human eye. Opt Lett 2002;27: 1537–1539.
6. Roorda A, Metha AB, Lennie P, Williams DR. Packing arrangement of the three cone classes in primate retina. Vision Res 2001;41:1291–1306.
7. Wolfing JI, Chung M, Carroll J, et al. High-resolution retinal imaging of cone-rod dystrophy. Ophthalmology 2006;113: 1014–1019.
8. Choi SS, Doble N, Hardy JL, et al. In vivo imaging of the photoreceptor mosaic in retinal dystrophies and correlations with visual function. Invest Ophthalmol Vis Sci 2006;47:2080–2092.
9. Kitaguchi Y, Bessho K, Yamaguchi T, et al. In vivo measurements of cone photoreceptor spacing in myopic eyes from images obtained by an adaptive optics fundus camera. Jpn J Ophthalmol 2007;51: 456–461.
10. Bennett AG, Rudnicka AR, Edgar DF. Improvements on Littmann's method of determining the size of retinal features by fundus photography. Graefes Arch Clin Exp Ophthalmol 1994;232: 361–367.
11. Oyagi T, Fujikado T, Hosohata J, et al. Foveal sensitivity and fixation stability before and after macular translocation with 360-degree retinotomy. Retina 2004;24:548–555.
12. Curcio CA, Sloan KR, Kalina RE, Hendrickson AE. Human photoreceptor topography. J Comp Neurol 1990;292:497–523.
13. Miller DT, Williams DR, Morris GM, Liang J. Images of cone photoreceptors in the living human eye. Vision Res 1996;36: 1067–1079.
14. Pircher M, Baumann B, Gotzinger E, Hitzenberger CK. Retinal cone mosaic imaged with transverse scanning optical coherence tomography. Opt Lett 2006;31:1821–1823.
15. Zawadzki RJ, Choi SS, Jones SM, et al. Adaptive optics-optical coherence tomography: optimizing visualization of microscopic retinal structures in three dimensions. J Opt Soc Am A Opt Image Sci Vis 2007;24:1373–1383.
16. Ojima Y, Hangai M, Sasahara M, et al. Three-dimensional imaging of the foveal photoreceptor layer in central serous chorioretinopathy using high-speed optical coherence tomography. Ophthalmology 2007;114:2197–2207.

Jpn J Ophthalmol 2008;52:386–392
© Japanese Ophthalmological Society 2008

DOI 10.1007/s10384-008-0568-0

LABORATORY INVESTIGATION

Changes in Muscle Fiber Size and in the Composition of Myosin Heavy Chain Isoforms of Rabbit Extraocular Rectus Muscle Following Recession Surgery

Sung Chul Park, Yun Taek Kim, Sun A Kim, and Sei Yeul Oh

Department of Ophthalmology, Samsung Medical Center, Sungkyunkwan University School of Medicine, Seoul, Republic of Korea

Abstract

Purpose: To assess the changes in the size of muscle fibers and the composition of myosin heavy chain (MyHC) isoforms in the global layer (GL) and the orbital layer (OL) of rabbit rectus extraocular muscle (EOM) after recession.

Methods: The right superior rectus muscles of two rabbits were harvested at 3 days or 1, 2, or 4 weeks after recession (eight rabbits in total). At each time point, one muscle was used for measuring the cross-sectional area of the muscle fibers and the other for identifying the composition of MyHC. The right superior rectus muscles of three additional naïve rabbits were used as controls.

Results: The mean cross-sectional area of the OL fibers did not change significantly. However, that of the GL fibers significantly decreased at 3 days ($P < 0.001$) and 1 week ($P = 0.024$) postoperatively, and increased thereafter to reach the control levels at 2 and 4 weeks postoperatively. Three days after surgery, the total MyHC content and the proportion of type IIb MyHC (MyHCIIb) plus EOM-specific MyHC (MyHCeom) decreased and remained at its lower level for 4 weeks.

Conclusions: Transient atrophy and regeneration were observed only in the GL, and the changes in the MyHCIIb plus MyHCeom appeared to be related to these changes. **Jpn J Ophthalmol** 2008;52:386–392
© Japanese Ophthalmological Society 2008

Key Words: extraocular muscle, global layer, myosin heavy chain, orbital layer, recession

Introduction

The extraocular muscles (EOMs) are unique skeletal muscles that perform highly coordinated and complex movements such as fast saccades, smooth slow pursuit and vergence movements, and fixation on a given position. The EOMs can be divided into two distinct parts, the orbital layer (OL) and the global layer (GL).[1–3] The OL lies along the EOM surface facing the orbital wall, and the GL faces the eyeball and is partially enclosed by the OL. The active pulley hypothesis suggests that the GL and the OL have distinctive roles in ocular motility.[4–6] The GL terminates at the myotendinous scleral insertion and acts directly on the globe to move the eye, whereas the OL branches off further posteriorly and penetrates a sheath of connective tissue that acts as a pulley controlling the plane of eye rotation.[4–6]

Myosin is the major contractile protein in skeletal muscles, and the relative myosin isoform composition determines the contractile and biochemical properties of each skeletal muscle.[7] Myosin heavy chain (MyHC) contains adenosine triphosphatase and an actin-binding site, and is believed to have the largest effect on the speed of contraction, contractility, and fatigue resistance of skeletal

Received: November 23, 2007 / Accepted: June 1, 2008
Correspondence and reprint requests to: Sei Yeul Oh, Department of Ophthalmology, Samsung Medical Center, Sungkyunkwan University School of Medicine, 50 Ilwon-dong, Kangnam-ku, Seoul 135-710, Republic of Korea
e-mail: syoh@skku.edu

Adaptive Optics Fundus Camera to Examine Localized Changes in the Photoreceptor Layer of the Fovea

Yoshiyuki Kitaguchi, MD,[1] Takashi Fujikado, MD,[1] Kenichiro Bessho, MD,[1] Hirokazu Sakaguchi, MD,[2] Fumi Gomi, MD,[2] Tatsuo Yamaguchi, MS,[3] Naoki Nakazawa, BE,[3] Toshifumi Mihashi, PhD,[3] Yasuo Tano, MD[2]

Purpose: To examine highly localized photoreceptor disruptions in the fovea by a high-resolution adaptive optics (AO) fundus camera combined with Fourier-domain optical coherence tomography (FD OCT).

Design: Observational case series.

Participants: Three eyes of 3 patients who showed dark foveal spots by slit-lamp biomicroscopy.

Methods: Three patients who reported metamorphopsia but showed no changes in the retina in conventional fundus photographs were examined. High-resolution retinal images were obtained with the AO fundus camera and by FD OCT. The images were compared with the findings obtained by standard clinical tests, including Amsler charts and fluorescein angiography (FA).

Main Outcome Measures: Quantitative measurements of the area of photoreceptor disruption.

Results: Slit-lamp biomicroscopy revealed an irregularly shaped dark spot in the fovea centralis but no changes in FA in the 3 cases. The photoreceptor mosaic was absent in a highly localized area of the fovea in the images obtained by the AO fundus camera, and the photoreceptor outer segment was absent or disturbed at the corresponding area by FD OCT in all 3 cases. The horizontal and vertical sizes of the area of disturbance of the photoreceptor mosaic in the AO images in the 3 eyes were 400×200 μm, 300×120 μm, and 300×200 μm. These sizes were comparable to the photoreceptor outer segment disturbances in the OCT images which were 330×150 μm, 280×100 μm, 200×150 μm, respectively.

Conclusions: Localized OS disturbances were able to be detected in eyes with a dark foveal spot by AO fundus camera 2-dimensionally and by FD OCT axially. The good correspondence of the sizes of the area of photoreceptor disturbances obtained by AO images to those by FD OCT images indicate that the AO images can be used to evaluate and follow the 2-dimensional area of focal changes of the photoreceptors in the fovea quantitatively.

Financial Disclosure(s): Proprietary or commercial disclosure may be found after the references.
Ophthalmology 2008;115:1771–1777 © 2008 by the American Academy of Ophthalmology.

With current advanced retinal imaging instruments, small focal changes of the retina can be detected and measured more accurately. These findings can help in determining the cause of unexplained visual symptoms and visual loss. For example, the retina of patients at the early phase of macular dystrophy appears ophthalmoscopically normal.[1–6] However, examination of optical coherence tomography (OCT) images showed that the retina was thinner at the macular area and that the decrease in thickness was correlated with the reduced visual acuity.[4] With additional improvements in the axial resolution by ultra–high-resolution OCT, several studies have shown a good correlation between the disruption of the photoreceptor inner segment/outer segment (IS/OS) junction and the decrease in visual acuity.[7–10] Ultra–high-resolution OCT, or Fourier-domain (FD) OCT, has an axial resolution of approximately 3 to 5 μm,[9–12] which is significantly better than the axial resolution of approximately 10 μm with the standard OCT. This increased resolution results in better delineation of the retinal architecture and helps in identifying pathologic changes in the microstructure of the retina, especially the photoreceptor layer.[9–11]

A disturbance of IS/OS junction has been reported in cases of postoperative retinal detachment, central serous chorioretinopathy, and retinal dystrophy.[7,8,10,11,13,14] Some studies have found a good correlation between the disturbance of IS/OS junction and the visual acuity.[4,7,10,11]

One problem with conventional OCT is its low transverse resolution. Generally, the transverse resolution of OCT is on the order of 20 μm, which exceeds the cone mosaic spacing of 5 to 10 μm. Two reasons for this limitation are the ocular aberrations and saccadic eye movements. The A-scan technologies adopted in OCT are not suited for obtaining transverse information in both the x- and y-directions in a short acquisition time, and obtaining motion-artifact–free 2-dimesional transverse images of the cone mosaic is not possible.[16]

Adaptive optic (AO) systems seem to be well suited to overcome these problems. An AO system consists of a wavefront sensor to measure ocular aberrations and a de-

ISSN 0161-6420/08/$–see front matter
doi:10.1016/j.ophtha.2008.03.026

formable mirror to compensate for these aberrations. Correcting the ocular aberrations with the AO system can improve the transverse resolution to less than 2 μm, which is necessary to image individual photoreceptors in the living retina.[16–20] Because transverse 2-dimensional images of the retina can be obtained with the AO system, precise detection and measurements of small lesions can be made. Thus, the AO images of patients with cone dystrophy have been reported to have a patchy configuration because of photoreceptor dropout.[21–23] The limitation of the AO system is its low axial resolution. The axial resolution of AO system is approximately 100 μm, even when it is coupled with a scanning laser ophthalmoscope.[19] It is even greater with conventional flood-illumination fundus photography.

Because of the complementary aspects of FD OCT and AO, that is, high axial resolution with FD OCT and high transverse resolution with the AO system, it theoretically would be valuable to combine both instruments to evaluate small focal photoreceptor disruptions. However, the authors have not found a publication that used both systems to compare the images obtained with FD OCT and those obtained with the AO system. The authors have developed a compact, clinically friendly AO fundus camera using a liquid crystal phase modulator. With this instrument, they have been able to show the increased cone spacing in myopic eyes.[24] The purpose of this study was to determine the cause of dark spots in the fovea of 3 patients with metamorphopsia. In all 3 patients, the fundus appeared ophthalmoscopically normal and the photographs obtained by conventional fundus photography also demonstrated normal results. These retinas were examined with their custom-built AO fundus camera, and the images were compared with the OCT images.

Patients and Methods

Patients

Three consecutive patients who reported metamorphopsia but whose photographs of the ocular fundus by standard fundus photography demonstrated normal results were studied. All patients had visited Osaka University Hospital between January and June 2006. The research protocol was approved by the Institutional Review Board of the Osaka University Medical School, and the procedures conformed to the tenets of the Declaration of Helsinki. After the nature and possible consequences of the study were explained, written informed consent was obtained from all patients.

Procedures

All patients underwent a comprehensive ophthalmologic examination, including the measurement of best-corrected visual acuity (BCVA), Amsler chart, fundus photography, and slit-lamp biomicroscopy of the fundus. They also underwent examinations by FD OCT (RTVue-100; Optovue, Inc., Fremont, CA) and a custom-built AO fundus camera.[24] All 3 patients also underwent fluorescein angiography (FA) and indocyanine green angiography (ICGA).

Adaptive Optic Fundus Camera

A detailed description of the custom-built AO fundus camera has been published.[24] The principle of this flood illumination AO fundus camera was similar to that reported by Roorda and Williams.[17] Briefly, the main components of the camera were a nematic liquid crystal phase modulator (X8267–12; Hamamatsu Photonics, Hamamatsu, Japan), a Hartmann-Shack wavefront sensor (28×28 lenslets; specially made by Topcon, Co., Tokyo, Japan), and a scientific charge-coupled device digital camera (C9100–02; Hamamatsu Photonics).

The wavefront sensor measured the ocular wavefront up to the eighth Zernike order, and the phase modulator compensated for the measured wavefront aberrations. The system also is equipped with coaxial, 8-degree–wide viewing optics to identify the location and orientation of the highly magnified retinal images being observed.

Topical tropicamide (0.5%) and phenylephrine (0.5%) were used to dilate the pupil and to paralyze the ciliary muscle. The retina was illuminated with a 2-ms flash (635-nm wavelength) from a xenon arc lamp, and a retinal image was obtained with a 6-mm–diameter exit pupil. The patient was instructed to fixate a designated location on a target. Frame averaging was performed using custom software (Topcon) to improve the quality of the image. Overlapping images were merged using Photoshop (Adobe Systems, Inc., San Jose, CA). To identify the fovea, a montage of the AO images was made and superimposed on the fundus photographs and the fundus projection of OCT images.

Case Reports

Patient 1. A 39-year-old man reported metamorphopsia in his left eye which began 3 months earlier. His BCVA was 20/15 in both eyes. Ophthalmoscopy showed that the ocular fundus appeared normal in both eyes (Fig 1A). Slit-lamp biomicroscopy showed an irregularly shaped dark spot in the fovea centralis of the left eye. Amsler chart examination showed a localized area of metamorphopsia just below the fixation point.

Fourier-domain OCT demonstrated a disturbance of the IS/OS junction and OS layer (between second and third line of FD OCT) of approximately 330 μm on the horizontal scan and 150 μm on the vertical scan. The external limiting membrane layer was intact (Fig 1B,C).

The AO image showed a dark area, that is, an absence of the cone mosaic, at the fovea just above the fixation point. The shape of dark area was geographic, and the size was approximately 350 μm horizontally and 160 μm vertically (Fig 1D–F).

Patient 2. A 39-year-old man reported blurred vision and metamorphopsia in his right eye of 2 years' duration. His BCVA was 20/60 in the right eye and 20/20 in the left eye. He had been diagnosed with keratoconus in his right eye, but his vision did not improve after wearing a hard contact lens.

The ocular fundus appeared normal in fundus photographs (Fig 2A). Slit-lamp biomicroscopy showed an abnormal reflex in the macula and an irregularly shaped dark spot in the fovea centralis of the right eye. Amsler chart examination showed a central scotoma. Fluorescein angiography and ICGA did not show any abnormal findings (Fig 2B).

Fourier-domain OCT demonstrated a defect in the OS layer in the fovea that was located just under the IS/OS layer. The size of the defect was 280 μm on the horizontal scan and 100 μm on the vertical scan. The IS/OS junction was preserved but the intensity was slightly lower. The external limiting membrane and the RPE layers appeared to be normal (Fig 2C,D).

The AO image indicated a disappearance of the cone mosaic at the fovea. The dark area was oval, and the size was 300 μm horizontally and 120 μm vertically (Fig 2E–G).

Patient 3. A 62-year-old man reported metamorphopsia in his left eye of 6 months' duration. His BCVA was 20/200 in the right eye and 20/22 in the left eye. No abnormality was found in the ocular fundus in the conventional fundus photographs (Fig 3A). Slit-lamp biomicroscopy showed an irregularly shaped dark spot in the fovea centralis of the left eye. Amsler chart examination indicated a localized area of metamorphopsia just below the fixation point. The FA and ICGA results were normal (Fig 3B).

Fourier-domain OCT demonstrated an elevation of the external limiting membrane. The photoreceptor OS and IS/OS junction were not detected over an area of 200 μm on the horizontal scan and 150 μm on the vertical scan (Fig 3C,D).

The AO image demonstrated the disappearance of the cone mosaic at the foveal zone. At the fovea centralis, a relatively high reflective area without cone mosaic was observed. The area of the absence of foveal cones was approximately 300 μm horizontally and 200 μm vertically (Fig 3E,F).

Results

All 3 patients had metamorphopsia unilaterally, and the BCVA ranged 20/200 to 20/15 in the affected eye. The Amsler chart examination showed localized metamorphopsia in 2 eyes and a central scotoma in 1 eye. The ocular fundus appeared to be normal in standard fundus photographs, but slit-lamp biomicroscopy revealed an irregularly shaped dark spot in the fovea centralis in the 3 cases. Fluorescein angiography and ICGA did not show any abnormal findings in any cases.

Fourier-domain OCT demonstrated an absence of the OS and IS/OS junction of the photoreceptors in 1 case and an absence or disturbance of the OS but preservation of the IS/OS junction in 2 cases. The AO images indicated the absence of the cone mosaic in the foveal zone in all 3 cases. The horizontal and vertical sizes of the area of the absence of the photoreceptor mosaic in the AO images in the 3 eyes (400×200 μm, 300×120 μm, and 300×200 μm) were comparable with the sizes of the photoreceptor OS disturbances in the OCT images (330×150 μm, 280×100 μm, 200×150 μm, respectively).

Discussion

This study examined the FD OCT and AO images in patients who showed localized disturbances in the photoreceptor layer. To the best of the authors' knowledge, this is the first study that compares the FD OCT and AO images in the same patient. A localized disappearance of the photoreceptor mosaic was observed in the photographs of the fovea obtained by the AO fundus camera in all 3 cases. The horizontal and vertical sizes of the area of the loss of the photoreceptor mosaic in the AO images were comparable with the area of the OS disturbance in the OCT images. In patient 3, the IS/OS junction and OS were also not detected, but in patients 1 and 2, the IS/OS line was preserved, although the intensity was slightly lower than normal. These results suggested that the dark area seen by slit-lamp biomicroscopy corresponded with an absence of the photoreceptor mosaic in the AO images and with the disturbed photoreceptor OS in the OCT images.

The origin of the high reflectance cone mosaic in the AO fundus camera is reported to be from both the IS/OS junction and the OS in the normal retina.[15] However, based on the results from patient 1, a possibility exists that the OS is more involved in the reflectance of photoreceptor mosaic than the IS/OS junction in the AO images. This hypothesis corresponds with the results of a recent report using AO OCT, in which the cone mosaic is observed clearly at the level of Verhoeff's membrane (the third blight line of FD OCT), where the tip of the cone photoreceptor OS is enveloped by microvilli.[25]

In patients with a macular hole, metamorphopsia is a frequently reported symptom. In the early stage of macular hole, morphologic changes are observed not only in the photoreceptor layer, but also in the inner retinal layers because of the tangential traction on the retinal surface. All of the patients reported metamorphopsia, but the lesion was confined to only the photoreceptor layer and was in a very restricted area in the fovea.

Recently, a new clinical entity termed *foveal spot* or *macular microhole* has been proposed.[26,27] In this lesion, the patient has a mildly reduced visual acuity, a central scotoma, and metamorphopsia, and ophthalmoscopy shows a foveal defect with a red appearance and well-defined margins. The size of the lesion is approximately 100 μm and seems to be intraretinal. Conventional OCT3 images (Stratus model 3000; Carl Zeiss Meditec, Humphrey Division, Dublin, CA) show an abnormality of the outer retina, a defect of retinal pigment epithelium, or both.[27] All 3 of the eyes had an apparently normal ocular fundus by conventional fundus photography, but slit-lamp biomicroscopy showed an irregularly shaped dark spot in the fovea centralis. Thus, the 3 eyes may be included in the category of macular microhole or foveal spot. The decrease in the visual acuity or an increase in the area of metamorphopsia should be reflected in the size of the dark area in AO fundus image, and thus may be helpful to evaluate the progression of a disease quantitatively.

The limitation of this study is that the fovea could not be resolved accurately with the AO system. The AO system allows a transverse resolution of 2 μm, but the photoreceptors in the fovea are smaller than the resolution limit.[16–20] Because of this, it is difficult to identify the individual cones in the fovea centralis in the AO images. However, because the dark area is not observed in the central fovea in normal eyes, the dark area at or around the central fovea can be assumed to be the area of photoreceptor loss or disruption.

In conclusion, the AO fundus camera can acquire 2-dimensional images of the retina with a resolution of approximately 2 μm. This resolution allows the detection of highly localized disturbances of the photoreceptor cells that can correlate with the high-resolution images obtained by FD OCT. Combining the AO fundus camera and FD OCT images can be valuable to assess photoreceptor disruptions, especially in eyes with a small focal foveal lesion. The findings in these 3 patients indicate that patients reporting metamorphopsia may have a localized disruption the of photoreceptor cells in the fovea.

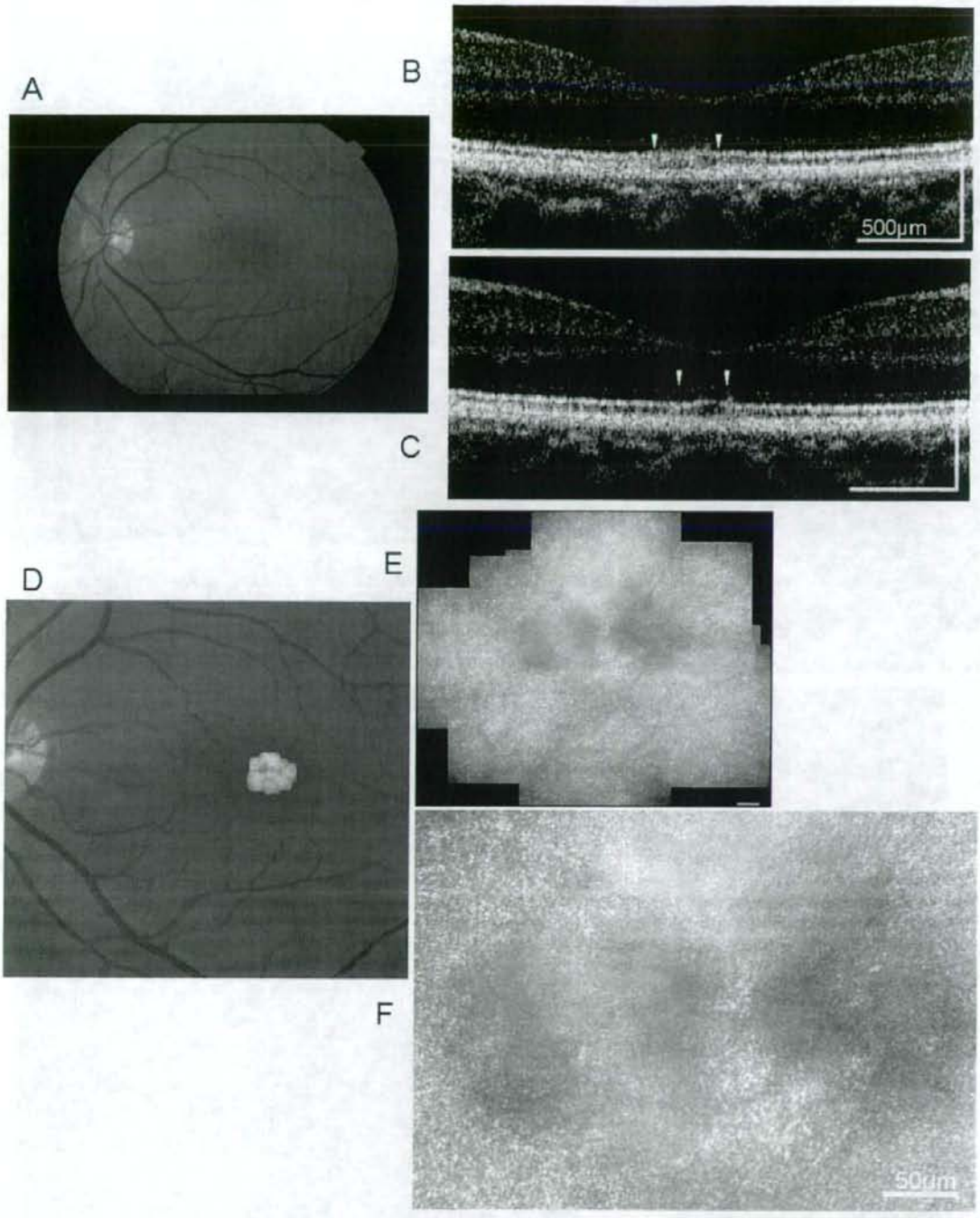

Figure 1. Images from the left eye of patient 1, who sought treatment for metamorphopsia. **A**, Fundus photograph showing normal appearance. **B**, Fourier-domain optical coherence tomography image (5-mm horizontal scan) demonstrating the disturbance of the inner segment/outer segment (IS/OS) junction and outer segment (OS) layer (between the second and third lines) for approximately 330 μm. **C**, Fourier-domain optical coherence tomography vertical scan showing the disturbance of the IS/OS junction and OS layer for approximately 150 μm. The arrowhead in **B** and **C** point to the area of IS/OS and OS disturbances. The horizontal bars in **B** and **C** represent 500 μm. **D**, Montage of adaptive optics (AO) image superimposed on the fundus photograph. **E**, Montage of adaptive optics image (low magnification). **F**, Magnified AO image of the fovea showing a dark area (disappearance of cone mosaic) at the fovea just above the fixation point. The shape of dark area was geographic and the size was approximately 350 μm horizontally and 180 μm vertically. The horizontal bars in **E** and **F** represent 50 μm.

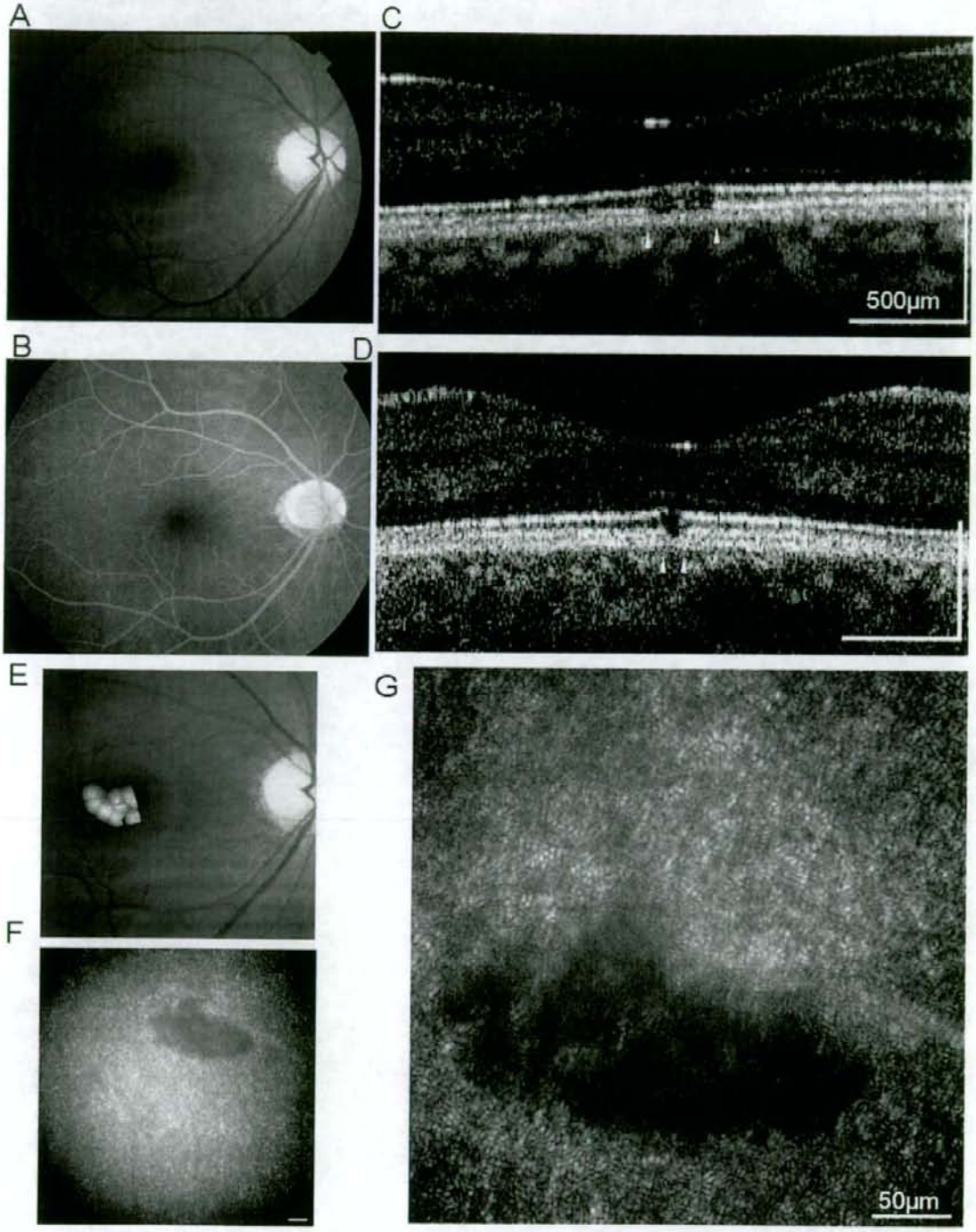

Figure 2. Images from the right eye of patient 2, who sought treatment for metamorphopsia. **A**, Fundus photograph showing that the retina appears to be normal. **B**, Early-phase fluorescein angiography image showing normal results. **C** and **D**, Fourier-domain optical coherence tomography images demonstrating a defect of outer segment (OS) layer in the fovea that was located just beneath the inner segment/OS junction. The size of the defect was (**C**) 280 μm on the horizontal scan and (**D**) 100 μm on the vertical scan. The IS/OS line was preserved but the intensity was slightly low. The arrowhead in **C** and **D** points to the area of OS defect. The horizontal bars in **C** and **D** represent 500 μm, and the vertical bars represent 200 μm. **E**, Montage of adaptive optics (AO) image superimposed on the fundus photograph. **F**, adaptive optics image (low magnification). **G**, Magnified AO image of the fovea showing a dark oval-shaped area (disappearance of cone mosaic) with a size of 300 μm horizontally and 120 μm vertically. The horizontal bars in **F** and **G** represent 50 μm.

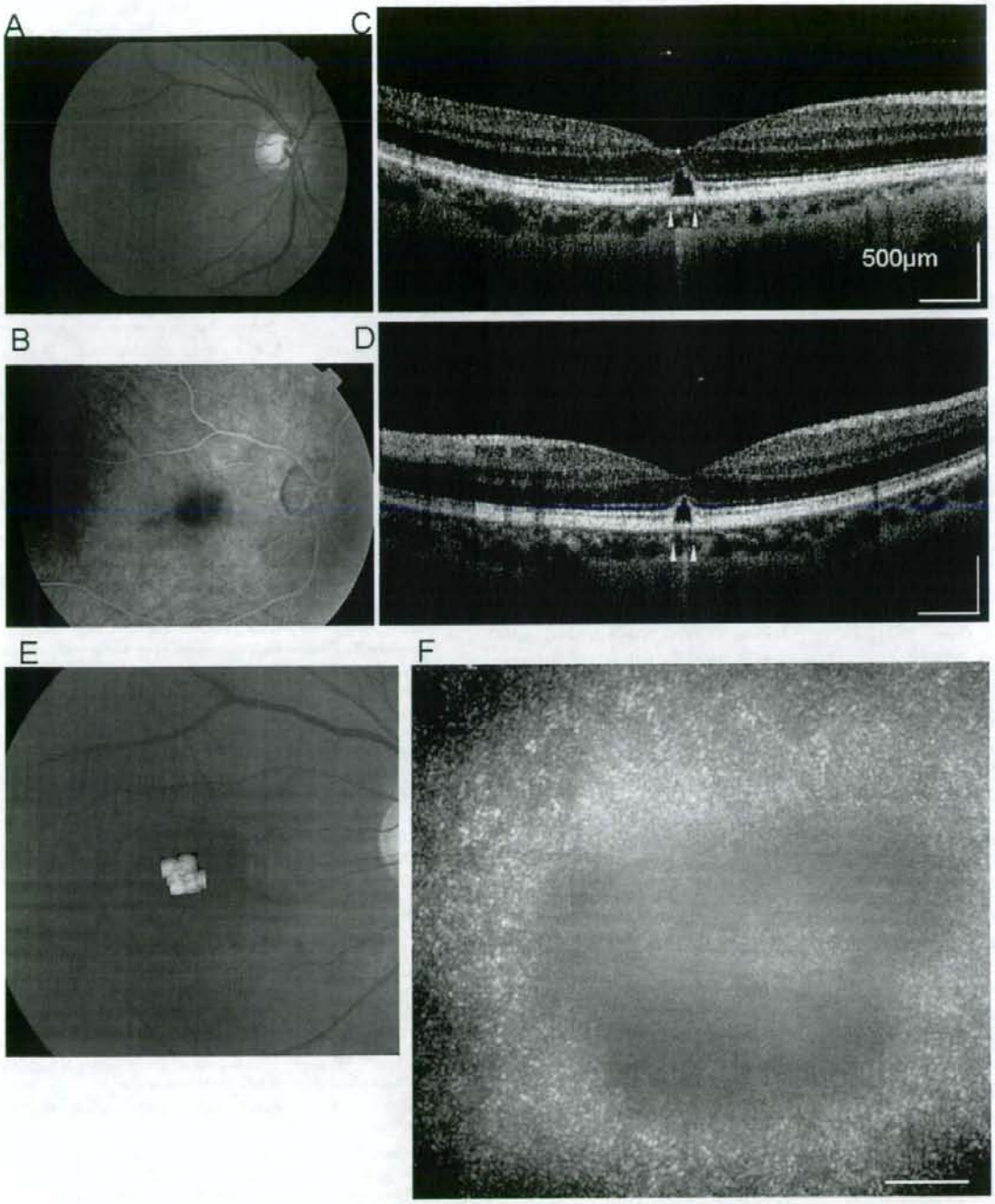

Figure 3. Images from the right eye of patient 3, who sought treatment for metamorphopsia. **A**, Fundus photograph showing normal appearance. **B**, Early-phase of fluorescein angiography image showing normal results. **C** and **D**, Fourier-domain optical coherence tomography images demonstrating the elevation of the external limiting membrane. Photoreceptor outer segment (OS) and inner segment/OS junction are not present in an area of (**C**) 200 μm on the horizontal scan and (**D**) 150 μm on the vertical scan. The arrowhead in **C** and **D** indicates the area of OS defect. The horizontal bars in **C** and **D** represent 500 μm, and the vertical bars represent 200 μm. **E**, Montage of adaptive optics (AO) image superimposed on the fundus photograph. **F**, Magnified image of AO image in the fovea demonstrating a dark oval-shaped area (disappearance of cone mosaic) with a size of 300 μm horizontally and 200 μm vertically. At the fovea centralis, a slightly high reflective area without cone mosaic was observed. The horizontal bars in **F** represent 50 μm.

References

1. Brockhurst RJ, Sandberg MA. Optical coherence tomography findings in occult macular dystrophy. Am J Ophthalmol 2007; 143:516–8.
2. Kondo M, Ito Y, Ueno S, et al. Foveal thickness in occult macular dystrophy. Am J Ophthalmol 2003;135:725–8.
3. Benhamou N, Souied EH, Zolf R, et al. Adult-onset foveomacular vitelliform dystrophy: a study by optical coherence tomography. Am J Ophthalmol 2003;135:362–7.
4. Sandberg MA, Brockhurst RJ, Gaudio AR, Berson EL. The association between visual acuity and central retinal thickness in retinitis pigmentosa. Invest Ophthalmol Vis Sci 2005;46: 3349–54.
5. Samsel A, Drobecka-Brydak E, Godowska-Brydak E, et al. Optical coherence tomography in Stargardt's dystrophy [in Polish]. Klin Oczna 2005;107:668–71.
6. Miyake Y, Horiguchi M, Tomita N, et al. Occult macular dystrophy. Am J Ophthalmol 1996;122:644–53.
7. Ergun E, Hermann B, Wirtitsch M, et al. Assessment of central visual function in Stargardt's disease/fundus flavimaculatus with ultrahigh-resolution optical coherence tomography. Invest Ophthalmol Vis Sci 2005;46:310–6.
8. Wirtitsch E, Ergun B, Hermann A, et al. Ultrahigh resolution optical coherence tomography in macular dystrophy. Am J Ophthalmol 2005;140:976–83.
9. Drexler W, Sattmann H, Hermann B, et al. Enhanced visualization of macular pathology with the use of ultrahigh-resolution optical coherence tomography. Arch Ophthalmol 2003;121:695–706.
10. Ojima Y, Hangai M, Sasahara M, et al. Three-dimensional imaging of the foveal photoreceptor layer in central serous chorioretinopathy using high-speed optical coherence tomography. Ophthalmology 2007;114:2197–207.
11. Schocket LS, Witkin AJ, Fujimoro JG, et al. Ultrahigh-resolution optical coherence tomography in patients with decreased visual acuity after retinal detachment repair. Ophthalmology 2006;113:666–72.
12. Alam S, Zawadski RJ, Choi S, et al. Clinical application of rapid serial Fourier-domain optical coherence tomography for macular imaging. Ophthalmology 2006;113:1425–31.
13. Piccolino FC, de la Longrais RR, Ravera G, et al. The foveal photoreceptor layer and visual acuity loss in central serous chorioretinopathy. Am J Ophthalmol 2005;139:87–99.
14. Iida T, Hagimura N, Sato T, Kishi S. Evaluation of central serous chorioretinopathy with optical coherence tomography. Am J Ophthalmol 2000;129:16–20.
15. Pircher M, Baumann B, Gotzinger E, Hitzenberger CK. Retinal cone mosaic imaged with transverse scanning optical coherence tomography. Optics Lett 2006;15:1821–3.
16. Liang J, Williams DR, Miller DT. Supernormal vision and high-resolution retinal imaging through adaptive optics. J Opt Soc Am A Opt Image Sci Vis 1997;14:2884–92.
17. Roorda A, Williams DR. The arrangement of the three cone classes in the living human eye. Nature 1999;397:520–2.
18. Roorda A, Williams DR. Optical fiber properties of individual human cones. J Vis 2002;2:404–12.
19. Roorda A, Romero-Borja F, Donnelly W III, et al. Adaptive optics scanning laser ophthalmoscopy. Opt Express [serial online] 2002;10:405–12. Available at: http://www.opticsexpress.org/abstract.cfm?id=68843. Accessed March 11, 2008.
20. Pallikaris A, Williams DR, Hofer H. The reflectance of single cones in the living human eye. Invest Ophthalmol Vis Sci 2003;44:4580–92.
21. Wolfing JI, Chung M, Carroll J, et al. High-resolution retinal imaging of cone-rod dystrophy. Ophthalmology 2006;113: 1014–9.
22. Choi SS, Double N, Hardy JL, et al. In vivo imaging of the photoreceptor mosaic in retinal dystrophies and correlations with visual function. Invest Ophthalmol Vis Sci 2006;47: 2080–92.
23. Duncan JL, Zhang Y, Gandhi J, et al. High-resolution imaging with adaptive optics in patients with inherited retinal degeneration. Invest Ophthalmol Vis Sci 2007;48:3283–91.
24. Kitaguchi Y, Bessho K, Yamaguchi T, et al. In vivo measurements of cone photoreceptor spacing in myopic eyes from images obtained by an adaptive optics fundus camera. Jpn J Ophthalmol 2007;51:456–61.
25. Zawadzki RJ, Choi SS, Jones SM, et al. Adaptive optics-optical coherence tomography: optimizing visualization of microscopic retinal structures in three dimensions. J Opt Soc Am A Opt Image Sci Vis 2007;24:1373–83.
26. Douglas RS, Duncan J, Brucker A, et al. Foveal spot: a report of thirteen patients. Retina 2003;23:348–53.
27. Zambarakji HJ, Schlottmann P, Tanner V, et al. Macular microholes: pathogenesis and natural history. Br J Ophthalmol 2005;89:189–93.

Footnotes and Financial Disclosures

Originally received: November 25, 2007.
Final revision: March 16, 2008.
Accepted: March 25, 2008.
Available online: May 16, 2008. Manuscript no. 2007-1518.

[1] Department of Applied Visual Science, Osaka University Graduate School of Medicine, Osaka, Japan.

[2] Department of Ophthalmology, Osaka University Graduate School of Medicine, Osaka, Japan.

[3] Topcon Research Institute, Tokyo, Japan.

Financial Disclosure(s):
The funding organization had no role in the design or conduct of this research.

Supported by the Ministry of Health, Labor and Welfare, Tokyo, Japan (Health Sciences Research grant no.: H19-sensory-001).

Tatsuo Yamaguchi, Naoki Nakazawa, and Toshifumi Mihashi are employees of Topcon.

Correspondence:
Takashi Fujikado, MD, Department of Applied Visual Science, Osaka University Graduate School of Medicine, 2-2 Yamadaoka, Suita, Osaka 565-0871, Japan. E-mail: fujikado@ophthal.med.osaka-u.ac.jp.

Potent Inhibition of Cicatricial Contraction in Proliferative Vitreoretinal Diseases by Statins

Shuhei Kawahara,[1] Yasuaki Hata,[1] Takeshi Kita,[1] Ryoichi Arita,[1] Muneki Miura,[1] Shintaro Nakao,[2] Yasutaka Mochizuki,[1] Hiroshi Enaida,[1] Tadahisa Kagimoto,[3] Yoshinobu Goto,[4] Ali Hafezi-Moghadam,[2] and Tatsuro Ishibashi[1]

OBJECTIVE—Despite tremendous progress in vitreoretinal surgery, certain postsurgical complications limit the success in the treatment of proliferative vitreoretinal diseases (PVDs), such as proliferative diabetic retinopathy (PDR) and proliferative vitreoretinopathy (PVR). One of the most significant complications is the cicatricial contraction of proliferative membranes, resulting in tractional retinal detachment and severe vision loss. Novel pharmaceutical approaches are thus urgently needed for the management of these vision-threatening diseases. In the current study, we investigated the inhibitory effects of statins on the progression of PVDs.

RESEARCH DESIGN AND METHODS—Human vitreous concentrations of transforming growth factor-β2 (TGF-β2) were measured by enzyme-linked immunosorbent assay. TGF-β2– and vitreous-dependent phosphorylation of myosin light chain (MLC), a downstream mediator of Rho-kinase pathway, and collagen gel contraction simulating cicatrical contraction were analyzed using cultured hyalocytes. Inhibitory effects of simvastatin on cicatrical contraction were assessed both in vitro and in vivo.

RESULTS—Human vitreous concentrations of TGF-β2 were significantly higher in the samples from patients with PVD compared with those without PVD. Simvastatin inhibited TGF-β2–dependent MLC phosphorylation and gel contraction in a dose- and time-dependent manner and was capable of inhibiting translocation of Rho protein to the plasma membrane in the presence of TGF-β2. Vitreous samples from patients with PVD enhanced MLC phosphorylation and gel contraction, whereas simvastatin almost completely inhibited these phenomena. Finally, intravitreal injection of simvastatin dose-dependently prevented the progression of diseased states in an in vivo model of PVR.

CONCLUSIONS—Statins might have therapeutic potential in the prevention of PVDs. ***Diabetes*** **57:2784–2793, 2008**

From the [1]Department of Ophthalmology, Graduate School of Medical Sciences, Kyushu University, Maidashi, Higashi-Ku, Fukuoka, Japan; the [2]Massachusetts Eye and Ear Infirmary, Department of Ophthalmology, Harvard Medical School, Boston, Massachusetts; [3]Aqumen Biopharmaceuticals, Tenjin, Chuo-Ku, Fukuoka, Japan; and the [4]Department of Occupational Therapy, Faculty of Rehabilitation, International University of Health and Welfare at Okawa, Enokizu, Okawa, Fukuoka, Japan.

Corresponding author: Yasuaki Hata, hatachan@med.kyushu-u.ac.jp.

Received 2 March 2007 and accepted 26 June 2008.

Published ahead of print at http://diabetes.diabetesjournals.org on 3 July 2008. DOI: 10.2337/db08-0302.

Proliferative vitreoretinal diseases (PVDs), such as proliferative diabetic retinopathy (PDR) and proliferative vitreoretinopathy (PVR), are common causes of severe vision loss (1). Surgical approaches for the treatment of these diseases have evolved significantly in the recent past, but the occurrence of postoperative complications, such as cicatricial contraction, limit the therapeutic success (2). Therefore, there is an urgent need for alternate pharmacological treatments of PVDs that can complement or potentially replace surgical intervention. In PDR and PVR, excessive wound healing and fibrosis induce the formation of proliferative membranes on the retinal surface. The proliferative membrane then extends into the vitreous and contracts, causing tractional detachment (3). The proliferative membrane consists of various cells, including hyalocytes, retinal pigment epithelial cells, glial cells, and fibroblast-like cells (4–7).

Hyalocytes morphologically resemble macrophages and are considered to originate from peripheral blood monocytes (8). Under physiological conditions, hyalocytes are mainly located in the cortical vitreous and are considered to maintain its transparency (9,10). Under pathological conditions, hyalocytes are thought to be critical in vitreoretinal interface diseases, such as idiopathic epiretinal membrane formation, macular hole, and diabetic macular edema (11). Hyalocytes in diabetic eyes are higher in number and of different shape compared with those in normal eyes (12).

Transforming growth factor-β (TGF-β) is pivotal to tissue fibrosis. Among the three isoforms of TGF-β, TGF-β2 is the predominant isoform in the vitreous (13,14). We and others have shown that TGF-β2 is overexpressed in the epiretinal membrane and vitreous of PDR and PVR patients and that its expression correlates with the presence of intraocular fibrosis (14–17). TGF-β2 modulates the differentiation of various cell types and is considered to increase the production of extracellular matrix, resulting in the formation and contraction of proliferative membranes (18,19). Thus, it is possible that the combination of hyalocytes and TGF-β2 may contribute to the pathogenesis of PVDs.

Statins, inhibitors of the 3-hydroxy-3-methyl-glutaryl (HMG)-CoA reductase, are widely used to reduce endogenous cholesterol synthesis and improve hypercholesterolemia (20). HMG-CoA reductase is an upstream enzyme in the mevalonate biosynthetic pathway that catalyzes the conversion of HMG-CoA into mevalonate and then, in a number of steps, into farnesylpyrophosphate (FPP), a precursor of cholesterol (21). By inhibiting HMG-CoA reductase, statins block the mevalonate pathway, resulting

in reduced synthesis of FFP and cholesterol. Statins are divided into three categories: the natural (i.e., lovastatin and pravastatin), the semisynthetic (i.e., simvastatin), and the synthetic (i.e., atorvastatin, fluvastatin, and cerivastatin). Statins decrease the risk for cardiovascular events even among high-risk individuals with coronary disease and diabetes (22). Moreover, statins may be useful in the treatment of other conditions, such as osteoporosis (23) and cancer growth and metastasis (24,25).

Another product of the mevalonate pathway is geranylgeranylpyrophosphate (GGPP), which is synthesized from FPP. Both FPP and GGPP are important isoprenoid intermediates and serve as lipid attachments for a variety of intracellular proteins to the plasma membrane, including the γ-subunit of heterotrimeric G-proteins and the small GTP-binding proteins, such as Ras and Rho, resulting in their activation (26). Rho translocation from the cytoplasm to the plasma membrane is dependent on geranylgeranylation (GGPP attachment), whereas Ras translocation is dependent on farnesylation (FPP attachment) (27). Rho in the plasma membrane is implicated in the cytoskeletal responses to extracellular signals and is converted to an active GDP-bound state (28). Rho-kinase, one of the effector molecules of Rho, is involved in a variety of cellular events related to cell morphology, adhesion, and motility (28–30), especially through phosphorylation of the myosin light chain (MLC). MLC phosphorylation induces actin-myosin interaction and, consequently, smooth muscle contraction and stress fiber formation in nonmuscle cells (31,32). Activation of the Rho/Rho-kinase pathway is therefore indispensable for smooth muscle contraction. GGPP is one of the downstream components of the mevalonate pathway and plays an important part in the Rho/Rho-kinase pathway activation. Thus, statins, which regulate the mevalonate pathway, also regulate the Rho/Rho-kinase pathway and, consequently, MLC phosphorylation.

Previously, we reported that the Rho-kinase pathway is involved in TGF-β2–induced MLC phosphorylation and contraction of hyalocyte-containing collagen gels and that hydroxyfasudil, a potent Rho-kinase inhibitor, significantly diminishes these TGF-β2–induced effects (18). In the present study, we investigate the regulatory effects of statins on TGF-β2– and vitreous-dependent MLC phosphorylation and contraction of hyalocyte-containing collagen gels and their therapeutic potential for prevention of PVDs in vivo.

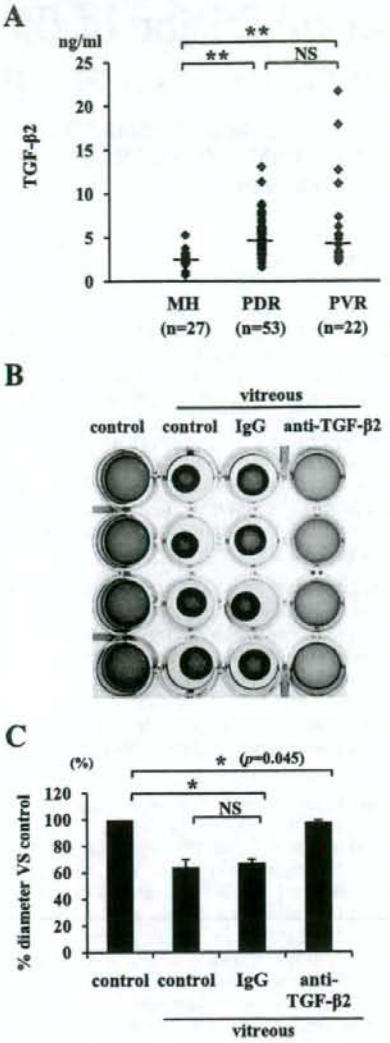

FIG. 1. TGF-β2 expression in the vitreous. *A*: **Vitreous samples were collected from patients with non-PVD (macular hole) and PVD (PDR and PVR). Concentrations of TGF-β2 in the vitreous were measured by enzyme-linked immunosorbent assay (macular hole, $n = 27$; PDR, $n = 53$; PVR, $n = 22$). $^{**}P < 0.01$ compared with macular hole.** *B*: **Hyalocytes were embedded in type I collagen gels ($n = 4$). After starvation and pretreatment with 1 μg/ml anti–TGF-β2 antibody or 1 μg/ml IgG for 1 h, the collagen gels were treated with vitreous samples from patients with PVD. Five days after the treatment, the gels were photographed.** *C*: **The diameter of the collagen gels was measured and expressed as percentage of the average diameter of the control group. $^{*}P < 0.05$.**

RESEARCH DESIGN AND METHODS

Reagents. Simvastatin, fluvastatin, pravastatin, and cerivastatin were purchased from CalBiochem (La Jolla, CA). Lovastatin was purchased from Funakoshi (Tokyo). Simvastatin was used as an active form after treatment with NaOH.

Vitreous samples and enzyme-linked immunosorbent assay. This study was carried out with approval from the Institutional Review Board and performed in accordance with the ethical standards of the 1989 Declaration of Helsinki. We obtained written informed consent from the patients. Vitreous samples were collected from patients who underwent pars plana vitrectomy because of non-PVD (macular hole) or PVD (PDR and PVR). Concentrations of TGF-β2 were measured by a human TGF-β2 immunoassay kit (R&D Systems, Minneapolis, MN).

Cell culture. Bovine hyalocytes were isolated as we previously reported (33). Cultured hyalocytes obtained between passages 5 and 7 were used in experiments.

Collagen gel contraction assay. The contraction assay was performed as we previously described (33). Type I collagen (Koken, Tokyo), a reconstitution buffer, hyalocytes suspension, and distilled water were mixed and added to a 24-multiwell plate (Nunc, Roskilde, Denmark). After 1-h pretreatment of vitreous samples with 1 μg/ml anti–TGF-β2 antibody (R&D Systems) or 1 μg/ml mouse IgG (Sigma-Aldrich) that was added for confirming the absence of nonspecific suppression of the gel contraction by anti–TGF-β2 antibody, the gels were treated with the vitreous samples (400 μl). The diameter of the collagen gel was measured at 5 days after the treatment. For quantitative purposes, contraction data are presented as the reduction in diameter of the collagen gels.

In the same way, collagen gels containing hyalocytes were starved, pretreated with statins for 24 h, and then treated with 3 ng/ml TGF-β2 (Sigma-Aldrich) or vitreous samples.

Western blot analysis. Total cell lysates were subjected to 15% SDS-PAGE, and the blots were incubated with an antibody against phosphorylated-MLC (*p*-MLC; 1:1,000; Santa Cruz Biotechnology, Santa Cruz, CA). Visualization was performed with an enhanced chemiluminesence (ECL; Amersham, Arlington

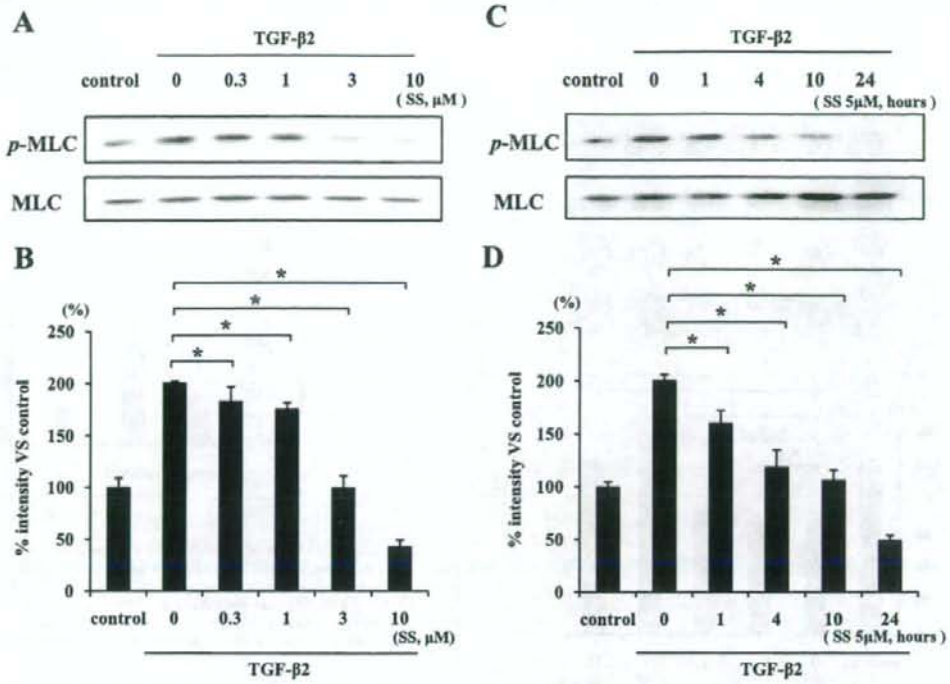

FIG. 2. Inhibitory effect of simvastatin on TGF-β2–dependent MLC phosphorylation. Hyalocytes were starved in Dulbecco's modified Eagle's medium containing 3% calf serum for 24 h. *A*: Hyalocytes were pretreated for 30 min with or without the indicated concentrations of simvastatin (0.3, 1, 3, and 10 μmol/l) and subsequently treated with 3 ng/ml TGF-β2 for 24 h. Total cell lysates were subjected to Western blot analysis with an antibody against *p*-MLC. Lane loading differences were normalized by reblotting the membranes with an antibody against MLC. *C*: Hyalocytes were pretreated with or without 5 μmol/l simvastatin for the indicated time (1, 4, 10, and 24 h) and subsequently treated with 3 ng/ml TGF-β2 for 24 h. *p*-MLC and MLC were also examined in the same way as in Fig. 1*A*. *B* and *D*: Signal intensity ratios (*p*-MLC to MLC) were expressed as percentage of control intensity ratio. *$P < 0.05$ compared with TGF-β2 alone.

Heights, IL) detection system. Lane loading differences were normalized by reblotting the membranes with an antibody against MLC (Santa Cruz) (1:1,000).

Plasma membrane proteins from the cells were isolated by Qproteome Plasma Membrane Protein kit (Qiagen, Hilden, Germany) and were subjected to Western blot analysis with an antibody against Rho (1:1,000; Upstate, Charlottesville, VA).

Counting viable cells in collagen gels. After 5 days of treatment, the collagen gels were dissolved by collagenase, and the cell suspension was collected. The viable cell number was counted with hemocytometer after trypan blue staining.

In vivo model of PVR. All experimental procedures using animals adhered to the Association for Research in Vision and Ophthalmology Resolution on the Use of Animals in Ophthalmic and Vision Research. We caused experimental PVR in rabbit eyes as previously described (34). Homologous conjunctival fibroblasts were prepared by harvesting the conjunctival tissue. Twenty eyes from 20 Dutch rabbits weighing 2–2.5 kg were assigned into three groups, and fibroblasts (100,000 cells) were injected into the right eye in each rabbit. Eyes in the first group (six eyes) were administered an intravitreal injection of 0.1 ml vehicle (balanced salt solution). Eyes in the second group (seven eyes) were administered an intravitreal injection of 0.1 ml vehicle containing simvastatin (5 μmol/l final intravitreal concentration). Eyes in the last group (seven eyes) were administered an intravitreal injection of 0.1 ml vehicle containing simvastatin (15 μmol/l final intravitreal concentration). The clinical observations were performed carefully as long as 28 days after surgery and categorized according with the PVR classification of Fastenberg et al. (35).

Electroretinography. Nine eyes from 10 Dutch rabbits weighing 2–2.5 kg were assigned into three groups. Eyes in the first group (three eyes) were administered an intravitreal injection of 0.1 ml vehicle. Eyes in the second group (three eyes) were administered an intravitreal injection of 0.1 ml vehicle containing simvastatin (5 μmol/l final intravitreal concentration). Eyes in the third group (three eyes) were administered an intravitreal injection of 0.1 ml vehicle containing simvastatin (15 μmol/l final intravitreal concentration). Electroretinogram was performed on day 28 as previously described (36).

Light microscopy. The eyes were enucleated and fixed in 4% paraformaldehyde on day 28. Whole eyes were cut approximately along the vertical meridian. Paraffin-embedded sections were stained with hematoxylin-eosin, and each section was examined using light microscopy.

TdT-dUTP terminal nick-end labeling assay. Apoptotic and potentially necrotic cell death was detected by TdT-dUTP terminal nick-end labeling (TUNEL). The eyes were fixed in 4% paraformaldehyde and embedded in paraffin. TUNEL staining was performed with the TdT Fluorescein in situ apoptosis detection kit (R&D Systems), according to the manufacturer's protocols. The sections were costained with propidium iodide (Molecular Probes, Eugene, OR) to observe the cell nuclei by fluorescence microscopy (KEYENCE, BIORAVO, and BZ-9000). As a TUNEL-positive control, we used the retina of rabbit PVR model on day 7 after the onset.

Transmission electron microscopy. The eyes were fixed in 1% glutaraldehyde and 1% paraformaldehyde in PBS. The specimens were postfixed in veronal acetate buffer osmium tetroxide (2%), dehydrated in ethanol and water, and embedded in Epon. Ultrathin sections were cut from blocks and mounted on copper grids. The specimens were observed with an electron microscope (H7650; Hitachi, Tokyo).

Statistical analysis. Statistical differences were assessed using nonparametric test (Kruskal-Wallis variance analysis) for the data of TGF-β2 concentrations and ANOVA for the other groups. P values <0.05 were considered significant. To adjust for inflated α-error due to multiple comparisons, the corrected significant P value was defined using the Bonferroni correction.

RESULTS

TGF-β2 in the vitreous and its impact on membrane contraction. The median TGF-β2 protein concentrations, 2.35 ng/ml (range 0.72–5.26) in macular hole ($n = 27$), 4.74 ng/ml (1.60–13.0) in PDR ($n = 53$), and 4.48 ng/ml (2.52–21.6) in PVR ($n = 22$) patients, were significantly higher in PDR or PVR patients than in patients with macular hole ($P < 0.01$) (Fig. 1*A*). The median TGF-β2 protein concen-

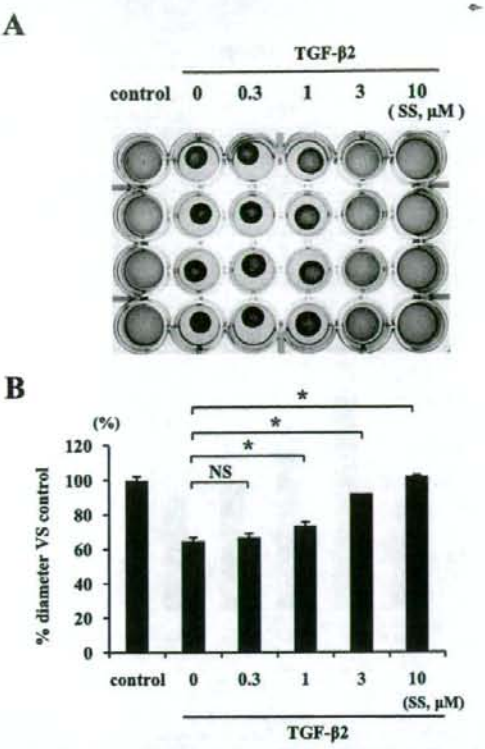

FIG. 3. The effect of simvastatin on TGF-β2–induced contraction of hyalocyte-containing collagen gels. Hyalocytes were embedded in type I collagen gels (n = 4). *A*: After starvation and pretreatment with indicated concentrations of simvastatin for 24 h, the collagen gels were stimulated with 3 ng/ml TGF-β2. Five days after the stimulation, the gels were photographed. *B*: The diameter of the collagen gels was measured and expressed as a percentage of the average diameter of control group. *P < 0.05; NS, not significant compared with TGF-β2 alone.

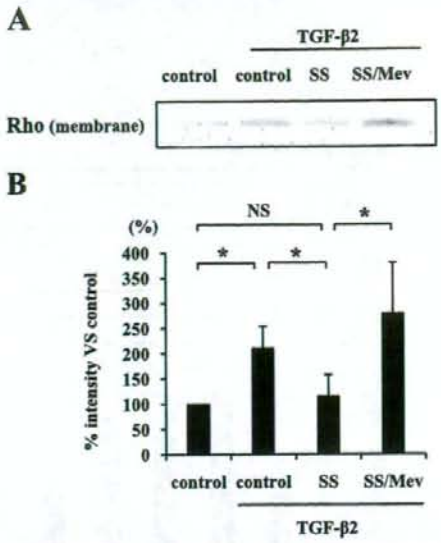

FIG. 4. Inhibitory effect of simvastatin on the Rho translocation to the plasma membrane. *A*: Hyalocytes were pretreated with 5 μmol/l simvastatin with or without mevalonate (Mev) and then treated with 3 ng/ml TGF-β2 for 24 h. Plasma membrane proteins were isolated and subjected to Western blot analysis with an antibody against Rho. *B*: Signal intensities were expressed as percentage of control intensity. *P < 0.05.

tration in the vitreous samples from patients with PDR or PVR showed no significant difference (P = 0.6).

Vitreous samples from patients with PVD and those containing nonspecific IgG induced significant contraction of hyalocyte-containing collagen gels (63 and 67% vs. control, respectively). In comparison, the vitreous-induced contraction was virtually suppressed by specific anti–TGF-β2 antibody (P < 0.05) (97% vs. control) (Fig. 1*B* and *C*), suggesting a key role for TGF-β2 in the vitreous-induced collagen gel contraction.

Role of simvastatin in TGF-β2–dependent MLC phosphorylation. TGF-β2 enhanced MLC phosphorylation to about two times that seen with control (Fig. 2*A* and *B*). TGF-β2–dependent MLC phosphorylation showed a significant reduction at 0.3 μmol/l simvastatin or higher concentrations (up to 10 μmol/l simvastatin) compared with TGF-β2 alone (P < 0.05). The level of MLC phosphorylation at 10 μmol/l simvastatin concentration was lower than in untreated control, suggesting that simvastatin at higher concentrations may block the constitutive level of MLC phosphorylation. Because 3 μmol/l simvastatin was sufficient to reverse the effect of TGF-β2 on MLC phosphorylation, we chose the slightly higher concentration of 5 μmol/l to study the time-dependent effect of simvastatin on TGF-β2–dependent MLC phosphorylation. Treatment of the hyalocytes with 5 μmol/l simvastatin for 1 h or longer (up to 24 h) significantly suppressed the MLC phosphorylation compared with TGF-β2 alone, and treatment with 5 μmol/l simvastatin for 24 h sufficiently suppressed the MLC phosphorylation below that of untreated control (Fig. 2*C* and *D*).

TGF-β2–dependent collagen gel contraction and its inhibition by simvastatin. The control gels showed no apparent contraction up to 5 days, whereas TGF-β2 caused substantial collagen gel contraction in a time-dependent manner in the first 5 days (57.6% vs. control). TGF-β2–dependent collagen gel contraction was significantly reduced by simvastatin starting at a concentration of 1 μmol/l, and the reduction was greater at 3 and 10 μmol/l (92 and 100% vs. control, respectively) (Fig. 3).

TGF-β2–dependent Rho translocation to the plasma membrane and its inhibition by simvastatin. TGF-β2 significantly enhanced the Rho translocation to the plasma membrane (P < 0.05), whereas simvastatin suppressed the translocation (Fig. 4*A* and *B*). However, the effect of simvastatin was reversed in the presence of 400 μmol/l mevalonate, a component of the mevalonate pathway. These findings suggest that simvastatin inhibits Rho/Rho kinase pathway by preventing Rho from translocating to the plasma membrane via inhibition of the mevalonate pathway.

Comparison of the effects of various statins on TGF-β2–dependent MLC phosphorylation and collagen gel contraction. Simvastatin and fluvastatin significantly suppressed TGF-β2–dependent MLC phosphorylation by hyalocytes, whereas pravastatin did not show an effect (Fig. 5*A* and *B*). In addition, simvastatin significantly suppressed MLC phosphorylation compared with fluvastatin (P < 0.05). Next, we compared the inhibitory effect of statins on the contraction of hyalocyte-containing collagen gels. Simvastatin and fluvastatin significantly suppressed TGF-β2–dependent contraction of collagen gel, whereas

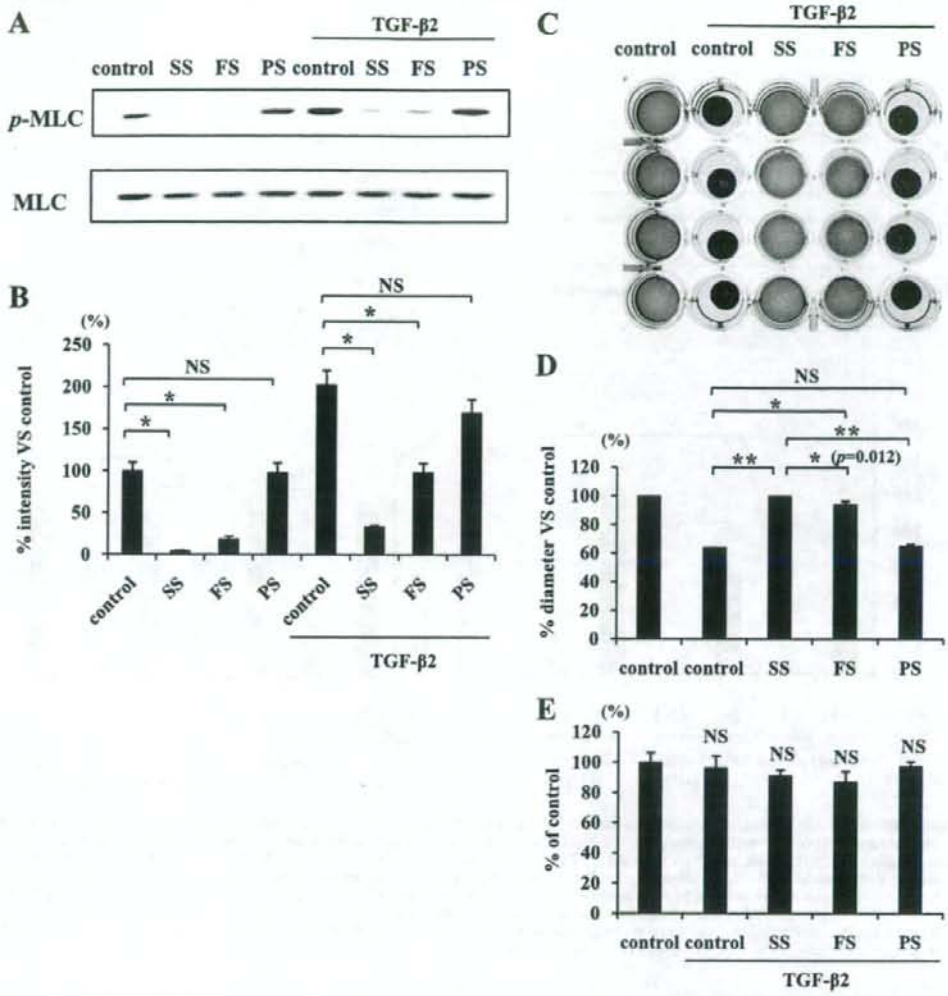

FIG. 5. Comparison of inhibitory effects of simvastatin, fluvastatin, and pravastatin on TGF-β2–dependent MLC phosphorylation and collagen gel contraction. *A*: Starved hyalocytes were pretreated with vehicle, 5 μmol/l simvastatin, fluvastatin, or pravastatin for 30 min and subsequently treated with or without 3 ng/ml TGF-β2 for 24 h. Total cell lysates were subjected to Western blot analysis with an antibody against *p*-MLC. Lane loading differences were normalized by reblotting the membranes with an antibody against MLC. *B*: Signal intensity ratios (*p*-MLC to MLC) were expressed as percentage of intensity ratio of vehicle alone. $^*P < 0.05$. *C*: Hyalocytes were embedded in type I collagen gels ($n = 4$). After starvation and pretreatment with vehicle, 5 μmol/l simvastatin, fluvastatin, or pravastatin for 24 h, the collagen gels were stimulated with 3 ng/ml TGF-β2. Five days after the stimulation, the gels were photographed. *D*: The diameter of the collagen gels was measured and expressed as percentage of the average diameter of control group. $^{**}P < 0.01$, $^*P < 0.05$; NS, not significant. *E*: The viable cell number in the collagen gels was counted to exclude the effect of cell growth or cytotoxicity on the collagen gel contraction or its inhibition. Five days after the treatment, the collagen gels were dissolved, and the cell suspension was collected. The viable cell number was counted with hemocytometer after trypan blue staining ($n = 4$; NS, not significant compared with control).

pravastatin did not show an effect (Fig. 5*C* and *D*). In addition, the inhibitory effect of simvastatin (100% vs. control) was significantly higher than that by fluvastatin (94% vs. control) ($P < 0.05$). To test whether cytokine and/or statin treatment affected the growth and/or viability of the cells in our experiments, we treated the collagen gels with collagenase and counted the number of viable cells. Both TGF-β2 and statins showed no significant effects on cell number in the three-dimensional collagen gels (Fig. 5*E*).

Impact of simvastatin on MLC phosphorylation and collagen gel contraction induced by vitreous samples from patients with PVD. Vitreous samples from patients with PVD caused a significantly larger enhancement of MLC phosphorylation than those from patients with non-PVD (Fig. 6*A* and *B*). Simvastatin (5 μmol/l) strongly attenuated the vitreous-induced MLC phosphorylation. Expression of GAPDH did not change after the treatment with simvastatin or stimulation with vitreous samples. However, total MLC increased in cells stimulated with the vitreous samples compared with cells without vitreous treatment, and the increase was larger in cells stimulated with vitreous samples from patients with PVD than those from patients without PVD. These increases in an amount of total MLC were suppressed by 5 μmol/l simvastatin.

The contraction of hyalocyte-containing collagen gels stimulated with the vitreous samples from patients with PVD was significantly larger compared with the contrac-

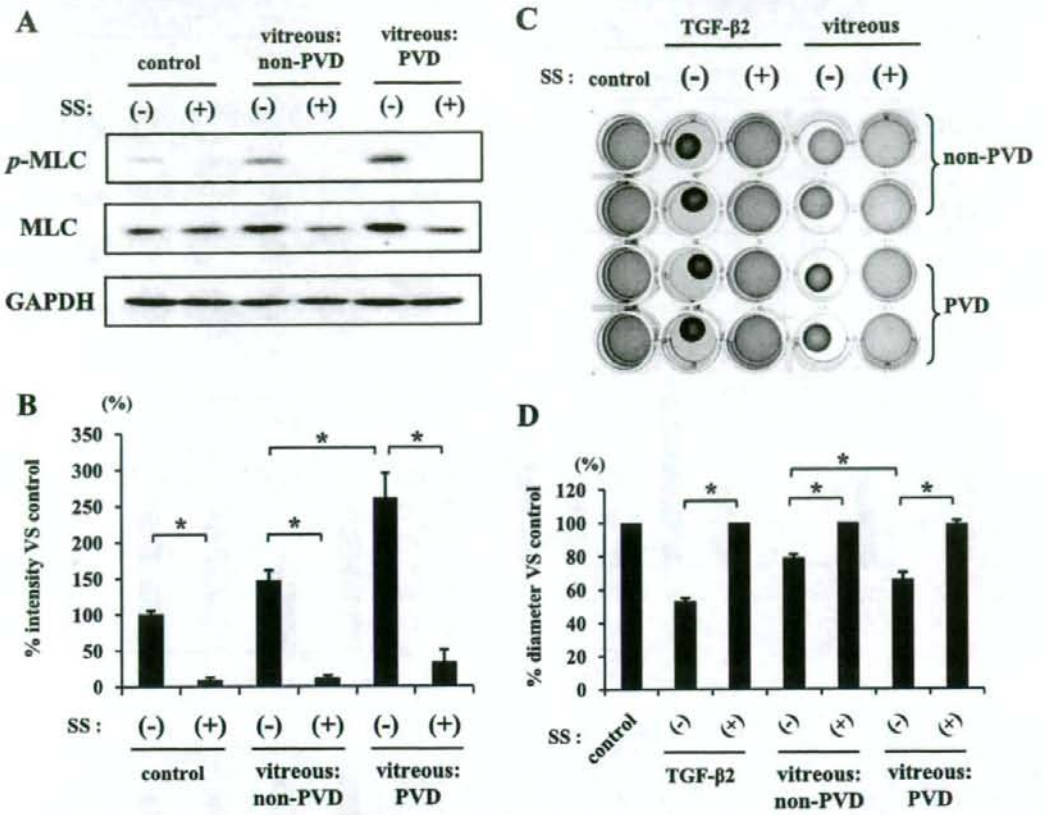

FIG. 6. Inhibitory effects of simvastatin on vitreous-induced MLC phosphorylation and contraction of hyalocyte-containing collagen gels. *A*: Starved hyalocytes were pretreated with 5 μmol/l simvastatin for 30 min and subsequently treated with or without 400 μl vitreous samples of non-PVD (macular hole) or PVD (PDR and PVR) for 24 h. Total cell lysates were subjected to Western blot analysis with an antibody against *p*-MLC. Lane loading differences were normalized by reblotting the membranes with an antibody against MLC and GAPDH. *B*: Signal intensity ratios (*p*-MLC to GAPDH) were expressed as percentage of control intensity ratio. *C*: Hyalocytes were embedded in type I collagen gels ($n = 4$). After starvation and pretreatment with 5 μmol/l simvastatin for 24 h, the collagen gels were stimulated with 400 μl vitreous samples of non-PVD or PVD. Five days after the stimulation, the gels were photographed. *D*: The diameter of the collagen gels was measured and expressed as percentage of the average diameter of the control group. *$P < 0.05$.

tion of the gels stimulated with vitreous samples from patients without PVD ($P < 0.05$) (Fig. 6*C* and *D*). We further examined the inhibitory effect of simvastatin on vitreous-dependent contraction of collagen gels and found that 5 μmol/l simvastatin suppressed the collagen gel contraction induced by vitreous samples even from patients with PVD.

Simvastatin inhibition of PVR development in vivo. The control eyes of rabbits injected with vehicle developed PVR and were accompanied by proliferative membrane formation and cicatricial contraction, resulting in tractional retinal detachment (Fig. 7*A*). In comparison, 5 and 15 μmol/l simvastatin (final intravitreal concentrations) significantly prevented PVR development (Fig. 7*C*). Simvastatin inhibited the contraction of the proliferative membrane, and the membranes in eyes treated with simvastatin were much thinner than those in vehicle-treated eyes (Fig. 7*B*). After simvastatin injections were stopped at day 7, the eyes treated with 5 μmol/l simvastatin developed a mild but significant PVR, whereas no significant PVR development was observed in the eyes treated with 15 μmol/l simvastatin.

Absence of apparent adverse effects of simvastatin in the retina. To evaluate the retinal function after intravitreal application of simvastatin, we performed electroretinography. The mean amplitude and latency of the 2Hz b wave in the eyes treated with 5 or 15 μmol/l simvastatin were 203.4 μV and 28.1 ms and 201.7 μV and 28.4 ms, respectively, and were not significantly different from those without any treatment or those of the vehicle-treated eyes (204.8 μV and 28.1 ms), suggesting that at these concentrations, simvastatin may not impede retinal function (Fig. 8*A*).

The histological structure of the retina in the eyes injected with simvastatin appeared normal when observed on day 28 (Fig. 8*B*, C).

In the retina of an experimental PVR used as a positive-control, apoptotic cells, which present TUNEL-positive staining (green), were detected in the inner nuclear layer and the outer nuclear layer (Fig. 8*D*). The eyes injected with simvastatin had no apparent TUNEL-positive staining in the retina when observed on day 28 (Fig. 8*E*).

The eyes injected with simvastatin had no apparent ultrastructual changes in internal limiting membrane,

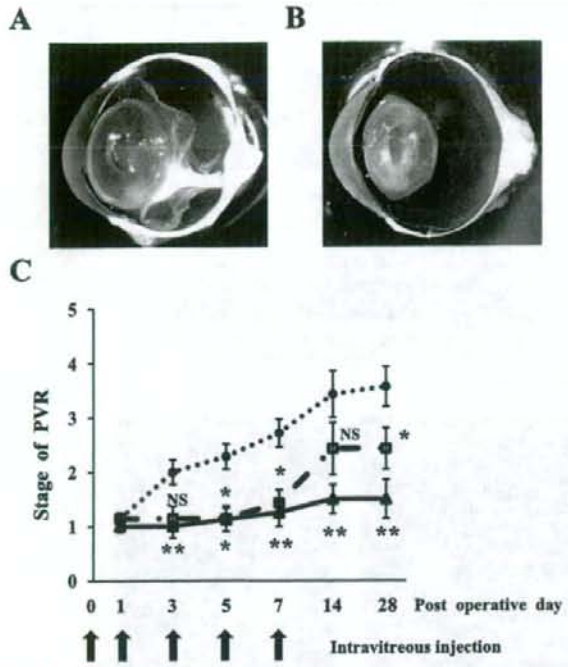

FIG. 7. Inhibitory effects of simvastatin on experimental PVR in rabbit eyes. Rabbits underwent vitrectomy and intravitreal injection of fibroblasts with and without simvastatin on day 0. The eyes were injected with same contents of simvastatin on days 1, 3, 5, and 7 and examined using indirect ophthalmoscope as long as 28 days after the surgery. *A*: A representative vehicle-injected eye with PVR in stage 5, 28 days after the surgery. Proliferative membranes were observed in the vitreous cavity, causing a traction to the retina and retinal detachment. *B*: A representative simvastatin-injected eye (15 μmol/l) with PVR in stage 1. A thin proliferative membrane was observed, however, there was no evidence of tractional retinal detachment. *C*: Clinical observations were categorized according to the PVR classification of Fastenberg et al. (35). Stage 1, intravitreal membrane; stage 2, focal traction, localized vascular changes, hyperemia, engorgement, dilation, and blood vessel elevation; stage 3, localized detachment of medullary ray; stage 4, extensive retinal detachment, total medullary ray detachment, and peripapillary retinal detachment; and stage 5, total retinal detachment. ●, vehicle; □, 5 μmol/l simvastatin; ▲, 15 μmol/l simvastatin. **$P < 0.01$, *$P < 0.05$; NS, not significant compared with vehicle.

nerve fiber layer, and ganglion cell layer (Fig. 8*G*) compared with the untreated control eyes (Fig. 8*F*). In other parts of the retina, such as inner and outer nuclear layers, photoreceptors, and retinal pigment epitheliums, there were also no apparent changes.

DISCUSSION

Blindness is a devastating consequence of PVDs such as PDR and PVR. Currently, the progression of these diseases cannot be effectively prevented, and the treatment options are limited to vitreoretinal surgery. An effective pharmacological treatment is thus urgently needed to complement or potentially replace the surgical intervention. In the current study, we show statins' novel function in inhibiting the Rho/Rho-kinase pathway, the contraction of collagen gel, and the progression of experimental PVR, suggesting the therapeutic potential of these compounds for the treatment of PVDs.

Various cytokines, such as TGF-β, connective tissue growth factor, interleukin-6, and platelet-derived growth factor (PDGF), are overexpressed in the vitreous and membranes associated with PDR and PVR, and they contribute to the pathogenesis of these diseases (15,37–40). Among these cytokines, TGF-β2 induces the transformation of retinal pigment epithelial cells or hyalocytes to myofibroblastic cells (18,41) and plays a key role in the formation and contraction of proliferative membranes. In this study, we confirmed the overexpression of TGF-β2 in the vitreous from patients with PVD (PDR and PVR) and showed that TGF-β2 inhibition strongly suppressed the vitreous-induced contraction of the collagen gels. This indicates the possibility that TGF-β2 is the dominant contributor to the contraction of proliferative membrane in the vitreous cavity. Thus, we focused on the role of TGF-β2 to investigate the mechanisms of membrane contraction. TGF-β2 enhanced MLC phosphorylation in hyalocytes that was responsible for the contraction of the hyalocyte-containing collagen gels. We showed that simvastatin suppressed TGF-β2–induced MLC phosphorylation and collagen gel contraction in a dose-dependent fashion by inhibiting GGPP-mediated translocation of Rho to the plasma membrane, whereas no signs of cytotoxicity were apparent.

Differences in the structural characteristics of statin cause different levels of lipophilicity and possibly of efficacies and also cytotoxicity. Pravastatin is strongly hydrophilic, and simvastatin is much more lipophilic than pravastatin (42). Fluvastatin is also more lipophilic than pravastatin; however, it is less lipophilic than simvastatin (43). Although our comparison of the inhibitory effects of various statins, simvastatin, fluvastatin, and pravastatin, revealed that simvastatin was more effective in reducing MLC phosphorylation than the other statins under the chosen experimental conditions, the results might vary at other time points or concentrations. Further examination is necessary to determine the order. Additionally, because cerivastatin is more lipophilic than simvastatin (44), we studied the effects of cerivastatin and simvastatin. Many hyalocytes treated with 5 μmol/l cerivastatin for 24 h shrank and detached from the culture plates, whereas the cells treated with 5 μmol/l simvastatin remained morphologically unchanged. However, at higher concentrations (>20 μmol/l), some hyalocyte shrinkage was observed even with simvastatin (data not shown). Cerivastatin is known to be cytotoxic and induce apoptosis (45). The morphological changes we observed in cerivastatin-treated hyalocytes in our study suggest that this drug may also be toxic to hyalocytes and promote their apoptosis. Because the lipophilicity of lovastatin is similar to that of simvastatin (42), we compared their effect and found the inhibitory effect of simvastatin on MLC phosphorylation and collagen gel contraction to be greater than that of 5 μmol/l lovastatin for 24 h (data not shown).

Vitreous samples from patients with PDR and PVR induced MLC phosphorylation and contraction of hyalocyte-containing collagen gels, which were effectively inhibited by simvastatin. It may appear surprising that not only vitreous samples from patients with PVD but also those from non-PVD patients induced MLC phosphorylation and collagen gel contraction. However, this might be explained by the fact that TGF-β2 is expressed in vitreous samples of patients with macular hole at high enough concentrations to induce the observed phenomena. The concentrations of TGF-β2 in vitreous samples from patients with PVD (PDR and PVR) were higher than in those from macular hole patients. Therefore, in a concentration-dependent manner, the inductions might be greater in the vitreous samples

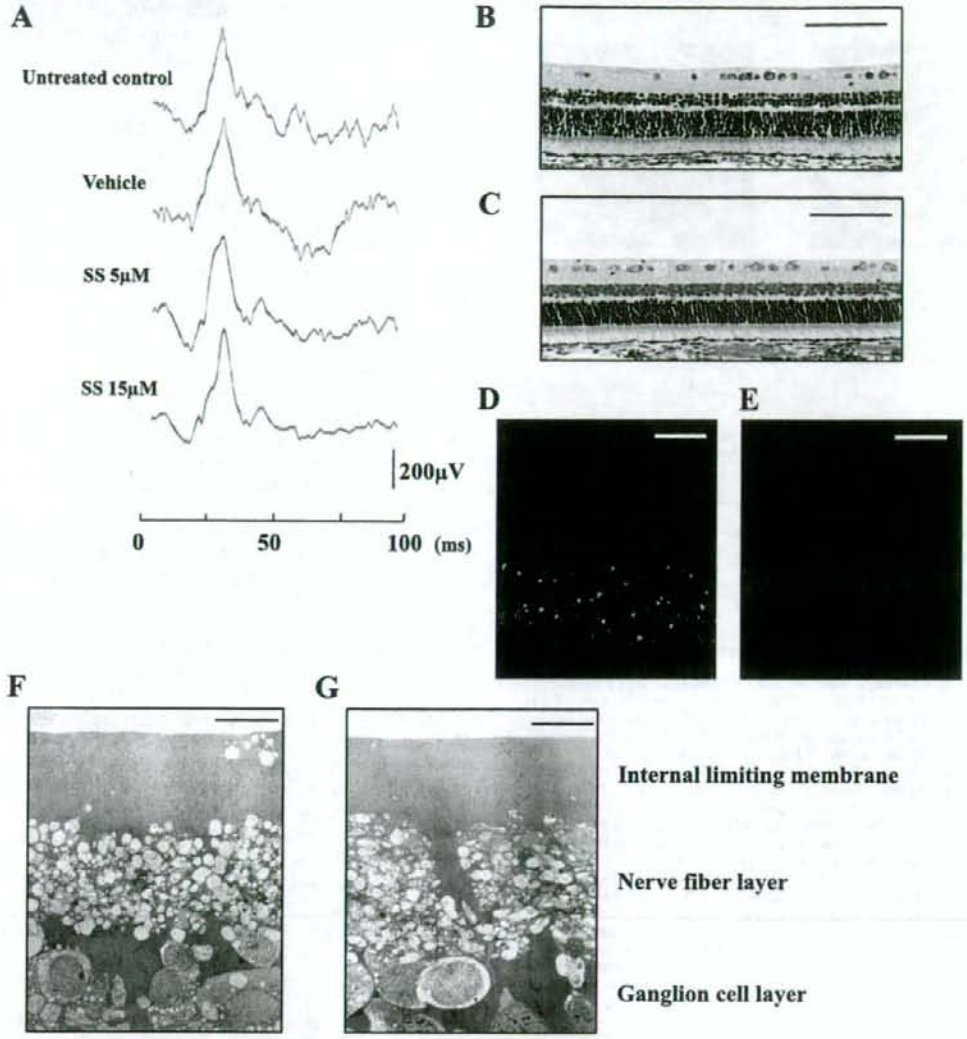

FIG. 8. Histological and physiological examinations of eyes injected with simvastatin. Rabbits received intravitreal injections of 0.1 ml vehicle or vehicle with simvastatin (final concentration of 5 or 15 μmol/l simvastatin) on days 0, 1, 3, 5, and 7. *A*: Electroretinograms on day 28. A flash stimulus of intensity 1.30 log cd.s/m^2 was superimposed on a background luminance of 1.15 log cd/m^2. Light microscopy of the rabbit eye without any treatment (*B*) and that of the eye injected with 15 μmol/l simvastatin (*C*). Scale bar = 100 μm. Apoptotic and potentially necrotic cell death detected by TUNEL in the section from positive control (rabbit PVR model on day 7 after its onset) (*D*) and in the section from the 15 μmol/l simvastatin-treated eye (*E*). Scale bar = 50 μm. Transmission electron microscopy of the rabbit eye without treatment (*F*) and that of the eye injected with 15 μmol/l simvastatin (*G*). Scale bar = 10 μm. (Please see http://dx.doi.org/10.2337/db08-0302 for a high-quality digital representation of this image.)

from patients with PVD than in those from patients without PVD. The concentrations of TGF-β2 in some vitreous samples from patients with macular hole were higher than those with PDR and PVR. However, the pathology of macular hole does not generally involve proliferative membrane formation and tractional retinal detachment. Occasionally, epiretinal membranes and retinal folds accompany macular hole. Retinal folds are considered to be caused by the contraction of the epiretinal membranes. TGF-β2 concentrations in vitreous samples from patients with macular hole may be high enough to induce contraction of proliferative membranes, however, because the epiretinal membrane in these patients does not extend into the vitreous and is very thin; the expression of TGF-β2 remains inconsequential.

MLC phosphorylation depends on the concentration of TGF-β2 (18); thus, the eyes with PVR having lower TGF-β2 concentrations might represent a less severe pathology, or remission, compared with those with higher TGF-β2 concentrations. The occurrence of tractional retinal detachment might depend on the presence or absence of proliferative membranes and the concentration of TGF-β2.

Although TGF-β2–stimulated hyalocytes showed no significant change in MLC expression, those stimulated with vitreous samples showed elevated MLC expression that was inhibited by simvastatin treatment. The vitreous in-

cludes various cytokines, released from retinal pigment epithelial cells, glial cells, macrophages, and other intravitreal cells (46). Thus, some cytokines other than TGF-β2 might elevate the expression of MLC. Among the cytokines found in the vitreous, insulin-like growth factor-I (IGF-I), PDGF, and members of the endothelin family have been shown to stimulate extracellular matrix contraction (18,47,48). This study reveals a key role for TGF-β2 in the pathology of PVDs; however, it is possible that other cytokines found in the vitreous might also be involved in MLC phosphorylation and contraction of hyalocyte-containing collagen gels. Because simvastatin almost completely inhibited the phenomena induced by vitreous samples, it might also inhibit the effect of the other cytokines, such as IGF-I, PDGF, and members of the endothelin family and unknowns, which might be exerted through the Rho/Rho-kinase pathway.

Simvastatin also prevented the development of PVR in vivo. Proliferative membranes in simvastatin-injected eyes, even if present, were very thin, whereas the membranes in vehicle injected eyes with PVR in stage 4 or 5 were thick. Thus, simvastatin might have also an inhibitory effect on the formation and growth of proliferative membranes in addition to the cicatricial contraction of proliferative membranes. However, after the end of the simvastatin injections, even in the groups treated with higher concentration of simvastatin (15 μmol/l) the development of PVR was not completely inhibited. This may be due to a short biological half-life time of the compound in the vitreous cavity. Therefore, to sustain a constant level of intravitreal simvastatin concentration, frequent injections or a slow release drug delivery system might be necessary.

Recent findings suggest that statins might have a number of beneficial effects in the eye. Although the applicability of statins on age-related macular degeneration is still under investigation (49), statins are shown to have protective effects on primary open-angle glaucoma, a major cause of blindness (50). The regulation of the intraocular pressure (IOP) within a physiological range is of great clinical importance. Statins are reported to downregulate the IOP by increasing aqueous humor outflow via the inhibition of Rho/Rho-kinase pathway in the trabecular meshwork and the ciliary body (50).

In conclusion, simvastatin potently inhibits the Rho/Rho-kinase pathway and thus might have therapeutic potential in the prevention of cicatricial contraction of proliferative membranes in vivo. This is the first report demonstrating the beneficial effects of simvastatin in inhibiting the development of PVR. Statins might provide a new strategy for the treatment and prevention of the development of PVDs in humans.

ACKNOWLEDGMENTS

S.N. has received a Research Fellowship Award from Bausch & Lomb and a Fellowship Award from the Japan Eye Bank Association. A.H.-M. has received National Institutes of Health Grants AI050775 and HL086933. This study has received Grants-in-Aid for Scientific Research 19592026, 18791283, and 18591925 from the Ministry of Education, Science, Sports and Culture, Japan; National Eye Institute Core Grant EY14104; and support from the Massachusetts Lions Eye Research Fund, the Marion W. and Edward F. Knight Age-Related and Macular Degeneration Fund, and Research to Prevent Blindness.

We acknowledge David Goodman (Pharmascience), Waichiro Katsuda, Tomoko Saeki, and Noriyuki Yoshida (Aqumen Biopharmaceuticals) for their excellent help.

REFERENCES

1. Pastor JC, de la Rua ER, Martin F: Proliferative vitreoretinopathy: risk factors and pathobiology. *Prog Retin Eye Res* 21:127–144, 2002
2. Pastor JC: Proliferative vitreoretinopathy: an overview. *Surv Ophthalmol* 43:3–18, 1998
3. Friedlander M: Fibrosis and diseases of the eye. *J Clin Invest* 117:576–586, 2007
4. Campochiaro PA: Pathogenic mechanisms in proliferative vitreoretinopathy. *Arch Ophthalmol* 115:237–241, 1997
5. Jerdan JA, Pepose JS, Michels RG, Hayashi H, de Bustros S, Sebag M, Glaser BM: Proliferative vitreoretinopathy membranes: an immunohistochemical study. *Ophthalmology* 96:801–810, 1989
6. Vinores SA, Campochiaro PA, Conway BP: Ultrastructural and electron-immunocytochemical characterization of cells in epiretinal membranes. *Invest Ophthalmol Vis Sci* 31:14–28, 1990
7. Machemer R, Laqua H: Pigment epithelium proliferation in retinal detachment (massive periretinal proliferation). *Am J Ophthalmol* 80:1–23, 1975
8. Lazarus HS, Hageman GS: In situ characterization of the human hyalocyte. *Arch Ophthalmol* 112:1356–1362, 1994
9. Grabner G, Boltz G, Forster O: Macrophage-like properties of human hyalocytes. *Invest Ophthalmol Vis Sci* 19:333–340, 1980
10. Mitchell CA, Risau W, Drexler HC: Regression of vessels in the tunica vasculosa lentis is initiated by coordinated endothelial apoptosis: a role for vascular endothelial growth factor as a survival factor for endothelium. *Dev Dyn* 213:322–333, 1998
11. Kampik A, Kenyon KR, Michels RG, Green WR, de la Cruz ZC: Epiretinal and vitreous membranes: comparative study of 56 cases. *Arch Ophthalmol* 99:1445–1454, 1981
12. Faulborn J, Dunker S, Bowald S: Diabetic vitreopathy: findings using the celloidin embedding technique. *Ophthalmologica* 212:369–376, 1998
13. Pfeffer BA, Flanders KC, Guerin CJ, Danielpour D, Anderson DH: Transforming growth factor beta 2 is the predominant isoform in the neural retina, retinal pigment epithelium-choroid and vitreous of the monkey eye. *Exp Eye Res* 59:323–333, 1994
14. Connor TB Jr, Roberts AB, Sporn MB, Danielpour D, Dart LL, Michels RG, de Bustros S, Enger C, Kato H, Lansing M: Correlation of fibrosis and transforming growth factor-beta type 2 levels in the eye. *J Clin Invest* 83:1661–1666, 1989
15. Kita T, Hata Y, Kano K, Miura M, Nakao S, Noda Y, Shimokawa H, Ishibashi T: Transforming growth factor-β2 and connective tissue growth factor in proliferative vitreoretinal diseases: possible involvement of hyalocytes and therapeutic potential of Rho kinase inhibitor. *Diabetes* 56:231–238, 2007
16. Ando A, Ueda M, Uyama M, Masu Y, Ito S: Enhancement of dedifferentiation and myoid differentiation of retinal pigment epithelial cells by platelet derived growth factor. *Br J Ophthalmol* 84:1306–1311, 2000
17. Vinores SA, Henderer JD, Mahlow J, Chiu C, Derevjanik NL, Larochelle W, Csaky C, Campochiaro PA: Isoforms of platelet-derived growth factor and its receptors in epiretinal membranes: immunolocalization to retinal pigmented epithelial cells. *Exp Eye Res* 60:607–619, 1995
18. Hirayama K, Hata Y, Noda Y, Miura M, Yamanaka I, Shimokawa H, Ishibashi T: The involvement of the rho-kinase pathway and its regulation in cytokine-induced collagen gel contraction by hyalocytes. *Invest Ophthalmol Vis Sci* 45:3896–3903, 2004
19. Jester JV, Ho-Chang J: Modulation of cultured corneal keratocyte phenotype by growth factors/cytokines control in vitro contractility and extracellular matrix contraction. *Exp Eye Res* 77:581–592, 2003
20. Molgaard J, von Schenck H, Olsson AG: Effects of simvastatin on plasma lipid, lipoprotein and apolipoprotein concentrations in hypercholesterolaemia. *Eur Heart J* 9:541–551, 1988
21. Graaf MR, Richel DJ, van Noorden CJ, Guchelaar HJ: Effects of statins and farnesyltransferase inhibitors on the development and progression of cancer. *Cancer Treat Rev* 30:609–641, 2004
22. MRC/BHF Heart Protection Study of cholesterol lowering with simvastatin in 20,536 high-risk individuals: a randomised placebo-controlled trial. *Lancet* 360:7–22, 2002
23. Coons JC: Hydroxymethylglutaryl-coenzyme A reductase inhibitors in osteoporosis management. *Ann Pharmacother* 36:326–330, 2002
24. Campbell MJ, Esserman LJ, Zhou Y, Shoemaker M, Lobo M, Borman E, Baehner F, Kumar AS, Adduci K, Marx C, Petricoin EF, Liotta LA, Winters M, Benz S, Benz CC: Breast cancer growth prevention by statins. *Cancer Res* 66:8707–8714, 2006